
Article:
Walaijai, Khanittha, Cavill, Stuart Alan orcid.org/0000-0002-1359-4958, Whitwood, Adrian C. et al. (2 more authors) (2020) Electrocatalytic proton reduction by a cobalt(III) hydride complex with phosphinopyridine PN ligands. Inorganic Chemistry. ISSN 0020-1669

https://doi.org/10.1021/acs.inorgchem.0c02505

Electrocatalytic proton reduction by a cobalt(III) hydride complex with phosphinopyridine PN ligands

Khanittha Walaijai,[a] Stuart A. Cavill,[b] Adrian C. Whitwood,[a] Richard E. Douthwaite,[a]* and Robin N. Perutz[a]*

[a] *Department of Chemistry, University of York, York YO10 5DD, UK*

[b] *Department of Physics, University of York, York YO10 5DD, UK*

ABSTRACT

Cobalt complexes with 2-(diisopropylphosphinomethyl)pyridine (**PN**) ligands have been synthesized with the aim of demonstrating electrocatalytic proton reduction to dihydrogen with a well-defined hydride complex of an Earth-abundant metal. Reactions of simple cobalt precursors with 2-(diisopropylphosphino-methyl)pyridine, (**PN**) yield $[Co^{II}(\mathbf{PN})_2(MeCN)][BF_4]_2$ **1**, $[Co^{III}(\mathbf{PN})_2(H)(MeCN)][PF_6]_2$ **2** and $[Co^{III}(\mathbf{PN})_2(H)(Cl)][PF_6]$ **3**. Complexes **1** and **3** have been characterized crystallographically. Unusually for a bidentate **PN** ligand, all three exhibit geometries with mutually trans phosphorus and nitrogen ligands. Complex **1** exhibits a distorted square-pyramidal geometry with an axial MeCN ligand in a low-spin electronic state. In complexes **2** and **3**, the PN ligands lie in a plane leaving the hydride trans to MeCN or chloride, respectively. The redox behavior of the three complexes has been studied by cyclic voltammetry at variable scan rates and by spectroelectrochemistry. A catalytic wave is observed in the presence of trifluoroacetic acid (TFA) at an applied potential close to the Co(II/I) couple of **1**. Bulk electrolysis of **1**, **2** or **3** at a potential of ca. –1.4 V vs $E(Fc^+/Fc)$ in the presence of TFA yields H_2 with Faradaic yields close to 100%. A catalytic mechanism is proposed in which the pyridine moiety of a **PN** ligand acts as a pendant proton donor following opening of the chelate ring. Additional mechanisms may also operate, especially in the presence of high acid concentration where speciation changes.

INTRODUCTION

Great advances have been made in developing catalysts for reduction of protons to hydrogen employing Earth-abundant elements.[1-5] Such reactions may involve molecular, semiconductor and/or enzymatic catalysts and may work via electrochemical or photochemical means or a combination of the two. However, synthetic catalysts cannot yet match the performance of hydrogenases in terms of a combination of high turnover frequency, catalyst longevity, low overpotential, and operation at neutral pH in aqueous solution.[6, 7] Solar fuel devices will need to improve performance if water splitting is to become a household reality.[8, 9] Our objective is to develop a proton-reduction system with an Earth-abundant metal, cobalt, in which we use a well-defined hydride complex as electrocatalyst.

Among molecular electrocatalysts, some of the best results have been obtained with cobalt and nickel complexes, especially those carrying a pendant base.[1, 3, 4, 10-21] While both homolytic and heterolytic mechanisms have been proposed for such catalysts, two features are invariably required, the ability to undergo proton-coupled electron transfer (PCET)[22-25] and the ability to form metal hydride complexes. Detection of metal hydride complexes associated with PCET is straightforward for heavier elements such as tungsten,[25, 26] but has proved challenging for the classic cobaloxime systems for catalytic hydrogen evolution;[3, 20, 27, 28] the nearest analogue[29] is $[Co^{III}H(Me_2NCH_2CH_2NMe_2)_2(OH_2)]^{2+}$. Most recently, Wiedner and Bullock have reported evidence for cobalt-hydride intermediates in related systems using variable scan rate cyclic voltammetry.[30] In contrast, cobalt hydride species can be detected straightforwardly for some cobalt phosphine complexes several of which are effective electrocatalysts or photocatalysts. Examples from both Co^{I} and Co^{III} oxidation states include $[CoH_2(bpy)(PR_3)_2]^+$, $[CoH(triphos)(MeCN)_2]^{2+}$, $CoH(PP)_2$, $[CoH_2(PP)]^+$, $[CpCoH(PP)]^+$, $CoH(PP_3)$, $[CoH_2(PP_3)]^+$,$Co(PNP)H_2$, $CoH_2(Bpin)(PN^{py}P)$ (where PR_3, PP, triphos, PP_3 represent mono, di, tri and tetradentate phosphines, respectively; PNP is an anionic pincer ligand and $PN^{py}P$ is a neutral pincer ligand, see Chart S1).[21, 27, 31-38] Hydride complexes of Co^{II} including Co(PNP)H, Co(POCOP)H, and $CoH(SiP_2)(PR_3)$ (POCOP and SiP_2 are anionic pincer ligands) may act as intermediates in the cycle for catalytic hydrogen evolution.[37, 39-42] Also relevant are dihydrogen complexes of Co^{I} phosphines $Co(SiP_3)(H_2)$, $Co(CCC)(PR_3)(H_2)$ (where SiP_3 represents an anionic tetradentate silyltris(phosphine) and CCC an anionic pincer bis(carbene)) since they may be converted to Co^{II} hydrides by deprotonation.[43, 44]

Comparison of the performance of different electrocatalysts for proton reduction to hydrogen has proved difficult until recently. However, the introduction of Foot Of The Wave (FOWA) analysis in conjunction with Tafel plots has given access to catalytic rate constants, k_{cat}

and the turnover frequency at zero overpotential and the maximum turnover frequency. These parameters which can be determined from measurement of cyclic voltammograms (CVs) as a function of scan rate, allow a standardized comparison of performance.[45-48] However, application of FOWA requires detailed knowledge of the catalytic mechanism.[48]

In this paper, we set out to synthesize and characterize some cobalt hydride complexes with bidentate phosphinopyridine ligands incorporating isopropyl substituents on phosphorus and test their electrocatalytic activity for proton reduction to molecular hydrogen. We show that the Co^{III} hydride complex requires initial 1e-reduction before the onset of catalysis.

EXPERIMENTAL SECTION

General Procedures and materials

All compounds were synthesized under an inert atmosphere of N_2 or Ar using standard Schlenk line and glove box techniques unless otherwise noted. Dry and deoxygenated solvents were prepared according to standard procedures. Hexane, THF, and ^{n}BuOH were dried by refluxing over Na under Ar. Acetonitrile, and MeOH were refluxed and dried over CaH_2. Deuterated solvents CD_3CN and CD_2Cl_2 were purchased from Sigma-Aldrich and dried over calcium hydride, prior to degassing by the freeze-pump-thaw technique (three times), and were stored under an Ar atmosphere in a glove box.

Solvents for general use were purchased from Fisher Scientific Ltd. All commercial chemicals were purchased from suppliers as follows: Sigma-Aldrich (ammonium hexafluorophosphate, cobalt(II) tetrafluoroborate hexahydrate, chlorodiisopropylphosphine, tetrabutylammonium hexafluorophosphate ($TBAPF_6$), trifluoroacetic acid, sodium borohydride), Merck (2-methylpyridine, 2.5 M n-butyllithium in hexane). All of these chemicals were used without further purification.

NMR spectra were recorded in tubes fitted with J. Young stopcocks on a Bruker AV500 (500 MHz) spectrometer at 298 K unless otherwise noted. The solvent signals were used as internal references for ^1H and $^{13}C\{^1H\}$ spectra and the chemical shifts were calibrated on residual solvent (CD_3CN δ_H = 1.94, δ_C = 1.39; CD_2Cl_2 δ_H = 5.32); $^{31}P\{^1H\}$, ^{19}F, and ^{15}N spectra are referenced against external standards with H_3PO_4 and $CFCl_3$ and pyridine, respectively.

The Evans method[49] was used to measure the magnetic moment for $[Co^{II}(\mathbf{PN})_2(MeCN)][BF_4]_2$ **1** in solution. A solution of **1** (0.4 ml, 0.0347 M) was prepared using the same stock solution as for the reference solvent (1.67% THF in CD_3CN) in the inner tube. The ^1H NMR chemical shifts of the reference compound (THF) in the two coaxial tubes were recorded on the Bruker AV500

spectrometer in the temperature range 298-330 K to obtain frequency shifts Δf (Hz). The magnetic moment was obtained from the slope of the Δf vs T^{-1} plot and the error determined from the line of best fit.

The solid-state magnetic measurement was made on a powder mounted in a polypropylene holder in a nitrogen filled drybox. The magnetization as a function of temperature, M(T), was measured between 20 and 300 K using a Quantum Design VSM-SQUID (MPMS) magnetometer. Measurements were performed in an applied field of 10 kOe for both zero-field cooled and field-cooled (40 kOe) conditions.

UV-Vis absorption spectra were recorded at ambient temperature on an Agilent 8453 spectrometer using quartz cuvettes fitted with a J. Young stopcock with 1 cm path length. The emission spectra were measured using a Hitachi F-4500 fluorimeter.

ESI mass spectra were recorded on a Bruker microTOF instrument.

Electrochemical and spectroelectrochemical studies were performed using a BASi Epsilon-EC potentiostat. EC-Lab software was used to process and analyze the data. All electrochemical experiments were performed in a three-neck single compartment electrochemical cell under an Ar atmosphere. All cyclic voltammetry (CV) was performed in an electrolyte of dried MeCN (7.5 mL) containing 0.1 M tetrabutylammonium hexafluorophosphate ($TBAPF_6$) degassed with Ar for 5 min. Stock solutions of trifluoroacetic acid were prepared under argon in the electrolyte used for electrochemical experiments in the presence of acid. A glassy carbon disk electrode (3 mm diameter) was used as the working electrode and the auxiliary electrode was a platinum wire. The pseudo reference electrode was a silver wire immersed in electrolyte solution and separated from the other electrodes by a Vycor frit. Ferrocene (2-3 mg) was added to the solution as an internal reference after electrolysis. The working electrode was thoroughly cleaned prior to each measurement by polishing with wet alumina powder on a polishing pad, then sonicating in millipore water for 3 min, and subsequently rinsed with millipore water and acetone prior to drying under a stream of N_2.

Spectroelectrochemistry was undertaken in MeCN in a three-electrode UV-Vis spectroelectrochemical quartz cuvette with a 1 mm path length (BASi). A Pt gauze was used as the working electrode, Pt wire as the counter electrode and a pseudo reference electrode (Ag wire immersed in CH_3CN containing 0.1 M $TBAPF_6$ electrolyte solution) separated from the solution by a Vycor frit. Changes in UV-Vis spectra during controlled-potential electrolysis were measured using an Agilent 8453 spectrometer.

All bulk electrolysis experiments for hydrogen evolution were performed in a 50 mL three-

neck round bottom flask containing 20 mL of electrolyte (0.1 M $TBAPF_6$ in MeCN) and complex catalyst (0.1 mM) under an Ar atmosphere. Carbon plates (10 mm x 10 mm x 1 mm) were used as working and counter electrodes. A silver wire immersed in acetonitrile containing 0.1 M ($TBAPF_6$) was used as the pseudo reference electrode, and ferrocene was added to the solution as an internal reference after electrolysis. The carbon plate working electrode was polished along all edges and faces using sandpaper with a few drops of millipore water prior to polishing with wet alumina powder on a polishing pad. The electrode was then rinsed with millipore water to eliminate alumina on the surface and sonicated in water for 30 min to remove all residual alumina. The electrode was rinsed with water and acetone (analytical grade) before drying under a stream of N_2.

Gas analysis was performed using a Shimadzu Corporation GC-2014 equipped with molecular sieve column and a thermal conductivity detector (TCD). Gas samples were analyzed with argon flow 20 mL min^{-1}, 90 ^oC column temperature and 120 ^oC detector temperature. Under these conditions, the retention time of H_2 is 1.0 min. 200 μL of gas was withdrawn from the headspace of the cell using a sample-lock gas-tight syringe. A calibration curve (SI) was built by using known quantities of 50% H_2/CO (SI). The peak area of H_2 for each complex was plotted against electrolysis time (SI). The peak area of H_2 at 1 h of electrolysis was fitted to the linear equation obtained through the calibration curve to obtain the experimental number of moles of H_2.

X-ray crystallography. Diffraction data were collected at 110 K using an Agilent SuperNova diffractometer with CuKα (λ = 1.54184 Å) or MoKα (λ = 0.71073 Å) radiation. The structures were solved and refined using Olex2.[50] Complex **1** was solved with the ShelXT [51] structure solution program using Intrinsic Phasing; complex **3** was solved with the Superflip[52] structure solution program using Charge Flipping Refinement and carried out with the ShelXL[51] refinement package using least squares minimization. The hydride was located by difference map and allowed to refine. Crystal data are listed in the SI.

Syntheses

2-(diisopropylphosphinomethyl)pyridine, (PN). The **PN** ligand was synthesized according to modified literature procedure.[53] A solution of 2.5 M ^{n}BuLi in hexane (11.0 mL, 1.1 mmol) was slowly added dropwise to a well-stirred solution of 2-methyl pyridine (2.33 g, 25 mmol) in dry and degassed THF (50 mL) at -78 ^oC. Upon adding ^{n}BuLi solution, the solution changed from colorless to yellow. The solution was warmed to room temperature and left to stir under an N_2 atmosphere for 4 h yielding a clear deep red solution. After cooling to –78 ^oC, this solution was slowly added via

cannula to a stirred solution of chlorodiisopropylphosphine in THF (50 mL) at –78 °C and was then vigorously stirred under N_2 while allowing it to warm up to room temperature. The reaction was quenched by adding MeOH (1.0 mL) to obtain a yellow-brown solution. All volatiles were subsequently removed at 60 °C under vacuum (ca. 1 mbar) to give a yellow-brown oil with a precipitate of LiCl. The mixture was purified by distillation at 105 °C under vacuum (0.01 mbar) to give **PN** as a yellow oil (3.10 g, 59% yield). ^{1}H and ^{13}C{^{1}H} NMR data were consistent with the literature see Figure 1 for numbering). Additionally ^{15}N data were recorded.[53]

^{1}H NMR (500 MHz, CD_3CN): δ8.40 (ddd, $^3J_{H,H}$ = 4.8, $^4J_{H,H}$ = 1.8, $^5J_{H,H}$ = 0.9 Hz, 1H, *H*$_1$), 7.60 (td, $^3J_{H,H}$ = 7.9, $^4J_{H,H}$ 2.0 Hz, 1H, *H*$_3$), 7.27 (ddt, $^3J_{H,H}$ = 7.9, $^4J_{H,H}$ = 1.1, $^5J_{H,H}$ = 1.0 Hz, 1H, *H*$_4$), 7.09 (ddd, $^3J_{H,H}$ = 7.4, $^4J_{H,H}$ = 5.0, $^5J_{H,H}$ = 1.1 Hz 1H, *H*$_2$), 2.96 (d, $^2J_{H,P}$ = 2.2 Hz, 2H, *H*$_6$), 1.79 (d of septets, $^2J_{H,P}$ = 1.7, $^3J_{H,H}$ = 7.1 Hz, 2H, *H*$_7$), 1.05 (dd, $^3J_{H,P}$ = 11.3, $^3J_{H,H}$ = 7.0 Hz, 6H, *H*$_8$), 1.02 (dd, $^3J_{H,P}$ = 13.5, $^3J_{H,H}$ = 7.2 Hz, 6H, *H*$_8$).

^{31}P{^{1}H} NMR (202.4 MHz, CD_3CN): δ12.4 (s).

^{13}C{^{1}H} NMR (125.7 MHz, CD_3CN): δ162.5 (d, $^2J_{C,P}$ = 8.9 Hz, *C*$_5$), 150.3(s, *C*$_1$), 137.4 (s, *C*$_3$), 124.9 (d, $^3J_{C,P}$ = 6.0 Hz, *C*$_4$), 122.0 (d, $^5J_{C,P}$ = 1.8 Hz, *C*$_2$), 33.5 (d, $^1J_{C,P}$ = 22.4 Hz ,*C*$_6$), 24.8 (d, $^1J_{C,P}$ = 14.7 Hz, *C*$_7$), 20.5 (d, $^2J_{C,P}$ = 15.3 Hz, *C*$_{8a}$), 19.7 (d, $^2J_{C,P}$ = 10.8 Hz, *C*$_{8b}$).

^{15}N-^{1}H HMBC (50.66 MHz, CD_3CN): δ1.6 (d, $^2J_{N,H}$ = 17 Hz).

Protonation of **PN** (9.9 mM) with 10.0 equiv trifluoroacetic acid (TFA) in CD_3CN generated a solution of [**PNH**][O_2CCF_3].

^{1}H NMR (500 MHz, CD_3CN): δ8.6 (ddd, $^3J_{H,H}$ = 5.15, $^4J_{H,H}$ = 1.8, $^5J_{H,H}$ = 0.9 Hz, 1H, *H*$_1$), 8.00 (td, $^3J_{H,H}$ = 7.7, $^4J_{H,H}$ 1.8 Hz, 1H, *H*$_3$), 7.60 (d, $^3J_{H,H}$ = 7.9 Hz, 1H, *H*$_4$), 7.52 (m, 1H, *H*$_2$), 4.01 (d, $^2J_{H,P}$ = 14.0 Hz, 2H, *H*$_6$), 2.80 (m, 2H, *H*$_7$), 1.34 (dd, $^3J_{H,P}$ = 19.4, $^3J_{H,H}$ = 7.2 Hz, 6H, *H*$_8$), 1.31 (dd, $^3J_{H,P}$ = 19.0, $^3J_{H,H}$ = 7.2 Hz, 6H, *H*$_8$).

^{31}P{^{1}H} NMR (202.4 MHz, CD_3CN): δ32.1 (s).

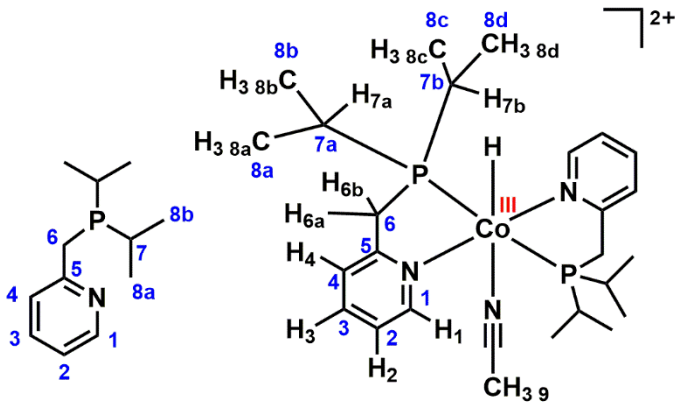

Figure 1. Atom labeling in **PN** and [Co^{III}(**PN**)$_2$(H)(MeCN)]$^{2+}$ **2.**

$[Co^{II}(PN)_2(MeCN)][BF_4]_2$ 1. A MeCN solution (5 mL) of the **PN** ligand (167 mg, 0.8 mmol) was added to a stirred MeCN (30 mL) solution of $[Co^{II}(CH_3CN)_6][BF_4]_2$ (192 mg, 0.4 mmol)[54] resulting in an immediate color change from pink to a deep red solution. This mixture was left to stir at room temperature under N_2 overnight prior to concentrating under vacuo to obtain a sticky deep red crude mixture. The crude product was then washed with dry ether with stirring for 30 min to give **1** as a red-orange solid (yield 249 mg, 0.36 mmol, 90%). Single crystals suitable for an X-ray diffraction study were grown by dissolving **1** in a small amount of CH_3CN and layering with THF to obtain deep red crystals.

ESI-MS (Acetone): m/z 238.5966 $[Co(\mathbf{PN})_2]^{2+}$, calcd for $[C_{24}H_{40}CoN_2P_2]^{2+}$ m/z 238.5971.

Magnetic moment in solution: 1.64±0.08 μB

Anal. Calcd for $C_{24}H_{40}B_2CoF_8N_2P_2$: C, 44.27; H, 6.19; N, 4.30; Found: C, 43.45; H, 6.12; N, 5.60.

$[Co^{III}(PN)_2(H)(MeCN)][PF_6]_2$ 2. Method A. $[Co^{II}(\mathbf{PN})_2(MeCN)][BF_4]_2$ (**1**) (56.7 mg, 0.082 mmol) was dissolved in MeOH (1.0 mL) with 1.3 equiv of $NaBH_4$ (3.8 mg, 0.10 mmol) and left to stir for 1 h. NH_4PF_6 (2.0 equiv., 25.6 mg, 0.157 mmol) was added as a solid resulting in precipitation of **2** as a yellow powder (25 mg, 0.031 mmol, 38% yield) which was separated from a deep brown solution by filtration, washed with a small amount of MeOH and dried with hexane and residual volatiles removed under vacuum. Atoms are numbered as in Figure 1.

Method B. A solution of $[Co^{III}(\mathbf{PN})_2(H)(Cl)][PF_6]$ (**3**) (21.2 mg, 0.032 mmol) (see below) in MeOH (5.0 mL) was charged with 10.0 equiv of trifluoroacetic acid (25 μl, 0.32 mmol). This solution was heated to 45 °C and was left to stir under N_2 for 6 h to obtain a greenish solution. All volatiles and excess CF_3COOH were removed under vacuum. A greenish powder was obtained and subsequently washed three times with a small amount of MeOH followed by hexane to afford a dry yellow solid as product (6 mg, 0.007 mmol 23% yield).

^{1}H NMR (500 MHz, CD_3CN): δ8.42 (d, $^3J_{H,H}$ = 5.8 Hz, 2H, Py-*H1*), 7.83 (td, $^3J_{H,H}$ = 7.8, $^4J_{H,H}$ 1.2 Hz, 2H, *H3*), 7.47 (d, $^3J_{H,H}$ = 7.8 Hz, 2H, *H4*), 7.30 (t, $^3J_{H,H}$ = 7.0 Hz, 2H, *H2*), 3.71 (d (br), $^2J_{H,H}$ = 17.6 Hz, 2H, *H6a or 6b*), 3.50 (d (br), $^2J_{H,H}$ = 17.5 Hz, 2H, *H6a or 6b*), 2.74 (broad m, simplifies to septet on decoupling ^{31}P, $^3J_{H,H}$ = 7.1, $^3J_{H,P} \approx$ 7.3 Hz, 2H, *H7a or 7b*), 2.54 (s, 3H, *H9*), 2.33 (broad m, simplifies to septet on decoupling ^{31}P $^3J_{H,H}$ = 7.0, $^3J_{H,P} \approx$ 6.9 Hz, 2H, *H7a or 7b*), 1.48 (virtual q, $^3J_{H,H}$ = 7.2, $^3J_{H,P}$ + $^5J_{H,P}$ = 7.4 Hz, 6H, *H8*), 1.26 (virtual q, $^3J_{H,H}$ = 7.0, $^3J_{H,P}$ + $^5J_{H,P}$ = 7.0 Hz, 6H, *H8*), 0.88 (virtual q, $^3J_{H,H}$ = 7.0, $^3J_{H,P}$ + $^5J_{H,P}$ = 7.0 Hz, 6H, *H8*), 0.68 (virtual q, $^3J_{H,H}$ = 7.2, $^3J_{H,P}$ + $^5J_{H,P}$ = 7.4 Hz, 6H, *H8*), –17.12 (t, $^3J_{H,P}$ = 54.3 Hz, 1H, Co-*H*).

$^{13}C\{^1H\}$ NMR (125.7 MHz,in CD_3CN): δ164. 6 (t, $^2J_{C,P} + ^4J_{C,P}$ = 3.2 Hz, *C5*), 157.7 (t, $^4J_{C,P} + ^6J_{C,P}$ = 4.7 Hz, *C1*), 141.1 (s, *C3*), 126.2 (t, $^3J_{C,P} + ^5J_{C,P}$ = 3.8 Hz, *C4*), 125.6 (s, *C2*), 35.4 (virtual t, $^1J_{C,P} + ^3J_{C,P}$ = 15.4 Hz, *C6*), 27.6 (virtual t, $^1J_{C,P} + ^3J_{C,P}$ = 6.7 Hz, *C7a or 7b*), 23.0 (s, *C7a or 7b*), 18.6 (s, *C8*), 18.3 (s, *C8*), 18.0 (s, *C8*), 17.6 (s, *C8*).

$^{31}P\{^1H\}$ NMR (202.4 MHz, in CD_3CN): δ72.4, (s, 2P), –144.6, (sep, 1P, PF_6^-)

ESI-MS (MeCN m/z +): 477.1994 $[Co(\mathbf{PN})_2]^+$, calcd for $[C_{24}H_{40}CoN_2P_2]^+$ 477.1993.

Anal. Calcd for $C_{24}H_{41}CoF_{12}N_2P_4$: C, 37.51; H, 5.38; N, 3.65; Found: C, 37.14; H, 5.27; N, 4.08.

$[Co^{II}(PN)_2Cl_2]$. Anhydrous $CoCl_2$ (16.3 mg, 0.125 mmol) was dissolved in dry and degassed n-BuOH (2.0 mL) and then added to a solution of **PN** ligand (0.0523 g, 0.25 mmol) in n-BuOH (3.0 mL). The solution was left to stir under N_2 for 3 h resulting in a dark red solution. This solution was then filtered via cannula to remove remaining $CoCl_2$. All volatiles were evaporated under vacuum to obtain a purple solid which was subsequently washed with diethyl ether and dried under vacuum to give the dichloro cobalt(II) complex, $[Co^{II}(\mathbf{PN})_2Cl_2]$, as a purple solid (67 mg, 0.122 mmol, 97% yield). This complex was characterized by CHN analysis.

Anal. Calcd for $C_{24}H_{40}Cl_2CoN_2P_2$: C, 52.57; H, 7.35; N, 5.11. Found: C, 52.56; H, 7.42; N, 4.95.

$[Co^{III}(PN)_2(H)(Cl)][PF_6]$ 3. Freshly prepared $[Co^{II}(\mathbf{PN})_2Cl_2]$ (67 mg, 0.12 mmol) was dissolved in MeOH (5 mL) and degassed by bubbling with N_2 for 10 min before adding $NaBH_4$ (5 mg, 0.132 mmol) as a solid. The mixture was stirred under N_2 for 1 h prior to adding solid NH_4PF_6 (20.4 mg, 0.125 mmol). After stirring for another hour at room temperature, $[Co^{III}(\mathbf{PN})_2(H)(Cl)][PF_6]$ **3** precipitated as an orange solid. This solid was washed with a small amount of MeOH and dried under vacuum to obtain an orange solid (39 mg, 0.059 mmol 49% yield). A single crystal of **3** suitable for X-ray crystallographic determination was obtained by recrystallization in acetone layered with hexane to give orange-red crystals.

^1H NMR (500 MHz, CD_3CN): δ8.89 (d, $^3J_{H,H}$ = 5.7 Hz, 2H, *H1*), 7.71 (td, $^3J_{H,H}$ = 7.8, $^4J_{H,H}$ 1.4 Hz, 2H, *H3*), 7.35 (d, $^3J_{H,H}$ = 7.8 Hz, 2H, *H4*), 7.18 (t br), $^3J_{H,H}$ = 6.7 Hz, 2H, *H2*), 3.58 (d br), $^2J_{H,H}$ = 17.2 Hz, 2H, *H6a or 6b*), 3.36 (d br), $^2J_{H,H}$ = 17.0 Hz, 2H, *H6a or 6b*), 2.59 (sep br), $^3J_{H,H}$ = 7.1, $^3J_{H,P}$ = 7.0 Hz, 2H, *H7a or 7b*), 2.25 (sep br), $^3J_{H,H}$ = 7.1, $^3J_{H,P}$ = 7.0 Hz, 2H, *H7a or 7b*), 1.62 (virtual q, $^3J_{H,H}$ = 7.1, $^3J_{H,P}$ + $^5J_{H,P}$ = 7.3 Hz, 6H, *H8*), 1.26 (virtual q, $^3J_{H,H}$ = 7.0, $^3J_{H,P}$ + $^5J_{H,P}$ = 6.8 Hz, 6H**,** *H8*), 0.94 (virtual q, $^3J_{H,H}$ = 7.0, $^3J_{H,P}$ + $^5J_{H,P}$ = 7.1 Hz, 6H, *H8*), 0.67 (virtual q, $^3J_{H,H}$ = 7.1, $^3J_{H,P}$ + $^5J_{H,P}$ = 7.3 Hz, 6H *H8*), –19.05 (t, $^3J_{H,P}$ = 59.7 Hz, 1H, Co-*H*).

$^{13}C\{^1H\}$ NMR (125.7 MHz, CD_3CN): δ164.9 (vt, $^2J_{C,P} + ^4J_{C,P}$ = 3.7 Hz, *C5*), 159.7 (t, $^4J_{C,P} + ^6J_{C,P}$ = 4.3 Hz, *C1*), 140.1 (s, *C3*), 125.0 (broad s, *C4*), 124.2 (s, *C2*), 36.0 (vt, $^1J_{C,P} + ^3J_{C,P}$ = 15.5 Hz, *C6*), 28.9 (vt, $^1J_{C,P}$

+ $^{3}J_{C,P}$ = 6.3 Hz, *C7a or 7b*), 22.9 (vt, $^{1}J_{C,P}$ + $^{3}J_{C,P}$ = 12.0 Hz, *C7a or 7b*), 19.1 (s, *C8*), 18.3 (s, *C8*), 18.2 (s, *C8*), 18.0 (s, *C8*).

$^{31}P\{^{1}H\}$ NMR (202.4 MHz, in CD_3CN): δ66.4, (s, 2P), –144.6, (sep, 1P, PF_6^-)

^{15}N-^{1}H HMBC (50.66 MHz, in CD_3CN): δ–96.5 (s).

ESI-MS (MeCN): m/z 513.1763 $[Co(\mathbf{PN})_2(H)(Cl))]^+$ (100 %), 477.1989 (M^+ - HCl, 70%) calcd for $[C_{24}H_{41}ClCoN_2P_2]^+$ 513.1760, $[C_{24}H_{40}CoN_2P_2]^+$ 477.1993.

Anal. Calcd for $C_{24}H_{41}ClCoF_6N_2P_3$: C, 43.75; H, 6.27; N, 4.25; found: C, 43.37; H, 6.03; N, 4.01

Reactivity of 1, 2 and 3 with TFA. Reactions were carried out in NMR tubes in CD_3CN solution under argon, typically with concentrations of complex of 5.4 mM or 9.9 mM and 10.0 equiv TFA. The UV-Vis titration experiments with TFA were performed by adding TFA to a solution of each complex in a UV-Vis cuvette fitted with a J. Young's stopcock and were measured by micropipette.

RESULTS AND DISCUSSION

Synthesis and characterization of cobalt complexes with bidentate P,N phosphinopyridine ligands. Reaction between 2-(diisopropylphosphinomethyl)pyridine (**PN**) and $[Co(MeCN)_6][BF_4]_2$ (Scheme 1) gave the Co(II) acetonitrile complex, $[Co^{II}(\mathbf{PN})_2(MeCN)][BF_4]_2$ (**1**) in high yield. Subsequent reaction between **1** and $NaBH_4$ followed by addition of NH_4PF_6 gave the cobalt(III) hydride complex $[Co^{III}(\mathbf{PN})_2(H)(MeCN)][PF_6]_2$ (**2**) which is soluble and stable in common solvents including MeOH, CH_3CN, THF and acetone under an Ar or N_2 atmosphere. The mechanism of conversion of **1** to **2** with $NaBH_4$ may proceed by reduction to Co(I), ($[Co(\mathbf{PN})_2]^+$) followed by protonation by NH_4PF_6 to obtain the monohydride complex. This pathway is analogous to the protonation of [CpCo(phosphine)$_2$] with NH_4PF_6 yielding isolable Co(III)-H complexes.[33] The orange monohydride complex $[Co^{III}(\mathbf{PN})_2(H)(Cl)][PF_6]_2$ (**3**) was prepared in 49% yield from reaction between $Co(\mathbf{PN})_2Cl_2$ and $NaBH_4$ using a similar method to that employed for **2**. [55] Complex **3** could be converted to **2** by reaction with trifluoroacetic acid in MeCN, providing an alternative, though lower yielding route to **2**.

Scheme 1. Preparation of cobalt complexes 1-3.

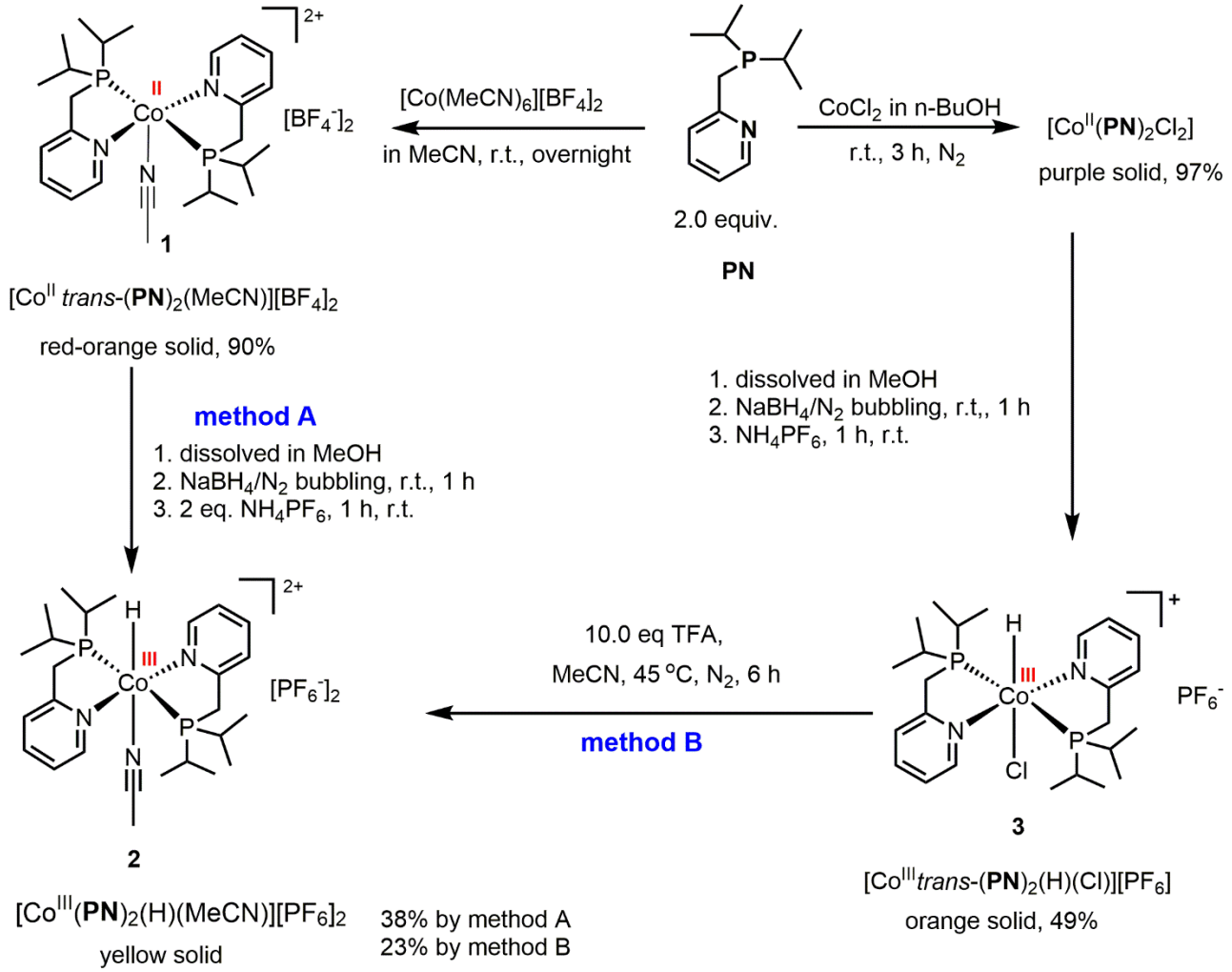

$Co^{II}(PN)_2(MeCN)][BF_4]_2$ (1). The red-orange acetonitrile cobalt(II) complex with **PN** ligands was identified as $[Co^{II}(\mathbf{PN})_2(MeCN)][BF_4]_2$ by crystallography (see below). (Paramagnetism prevented acquisition of NMR data for characterization.) Elemental analysis determined after drying under vacuum for 3 days yielded experimental values corresponding to partial loss of MeCN. Similarly, the ESI mass spectrum (m/z 238.5966) corresponded to $[Co(\mathbf{PN})_2]^{2+}$. The magnetic moment in CD_3CN solution was determined by the Evans method between 298 and 330 K as 1.64 $\pm$ 0.08 μ_B using THF as a reference. This value is consistent with one unpaired electron in a low spin d^7 complex as found for some $Co^{II}P_4$ complexes (Figure S2).[56] By using the temperature dependence of the magnetic susceptibility, contributions from diamagnetism and temperature dependent paramagnetism were eliminated. The solid state magnetic susceptibility of **1** varied almost linearly with T^{-1} yielding values of the magnetic moment of 2.07 μ_B at 30 K and 1.93 μ_B at

300 K, consistent with a low spin electronic state (Figure S2). The low spin electron configuration may moderate the lability of the **PN** ligands.

A deep red single crystal grown from CH_3CN/THF proved suitable for X-ray crystallographic determination. The crystal structure (Figure 2) showed five-coordinate cobalt(II) with the two **PN** ligands and one nitrogen atom from an acetonitrile ligand forming a distorted square pyramid. The two phosphinopyridine ligands lie in the equatorial plane with acetonitrile in an axial position. The structure exhibits crystallographic C_2 symmetry such that the two phosphorus atoms of the **PN** ligands lie trans to each other and the two N atoms are also mutually trans to one another. The majority of literature complexes with two phosphinopyridine ligands adopt a configuration with mutually cis phosphorus atoms and cis N atoms,[57,58,59] while one ruthenium complex exhibits cis P and trans N atoms.[58] Specifically for cobalt, the structurally related phosphinoamino ligands such as $Ph_2PC_2H_4NH_2$, $Me_2PC_2H_4NH_2$, and $Me_2PC_3H_6NH_2$ also exhibit mutually cis configurations.[60-62] We have found no literature examples of phosphinopyridine complexes of cobalt with mutually trans phosphorus and trans nitrogen ligand configurations.

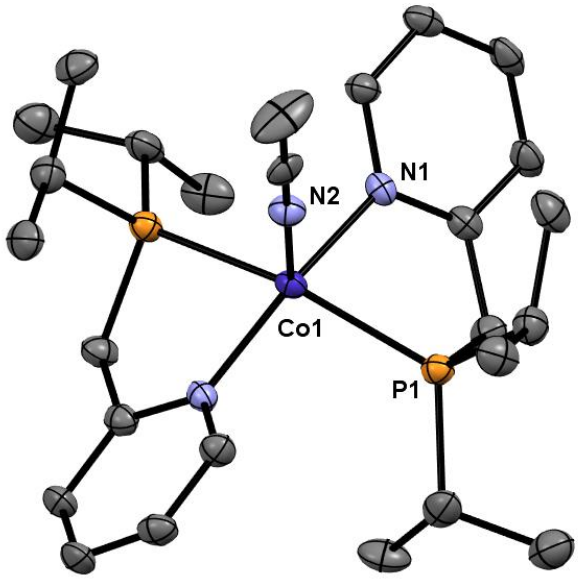

Figure 2. Molecular structure of the cation of $[Co^{II}(\mathbf{PN})_2(MeCN)][BF_4]_2$ (**1**). All hydrogen atoms and BF_4^- are omitted for clarity. Thermal ellipsoids are shown at the 50% probability level. Co-N1 1.967(6), Co-N2 2.034(9), Co-P1 2.2621(18) Å, N1-Co-N1´ 166.8(4), P1-Co-P1´ 160.67(12), N1-Co-N2 96.58(19), N1-Co-P1 81.53(17), N1-Co-P1´ 96.25(17), N2-Co-P1 99.67(6)°.

$[Co^{III}(PN)_2(H)(MeCN)][PF_6]_2$ (**2**). The cobalt(III) monohydride (**2**) was identified by NMR spectroscopy, elemental analysis and ESI mass spectrometry. NMR techniques included ^1H, $^1H\{^{31}P\}$, $^{13}C\{^1H\}$, ^{13}C-DEPT, $^{31}P\{^1H\}$ spectroscopy and 2D NMR correlation experiments. The signals in the ^1H and $^{31}P\{^1H\}$ NMR spectra of **2** are sharp and well-resolved, consistent with a low spin d^6 complex. There are four aromatic resonances and two resonances for the CH_2 group of the ligand. The four

methyl and two CH resonances of the isopropyl group all exhibit virtual coupling to phosphorus (Figures S10-S21).[63] The number of resonances and the virtual coupling indicate a chiral complex with C_2 symmetry and mutually trans phosphorus ligands. The hydride ligand appears as a triplet at δ–17.12 ($^3J_{H,P}$ = 54.3 Hz). Comparison with $^1H\{^{31}P\}$ NMR spectra confirmed the identification of H-P couplings. To identify a coordinated MeCN peak of this complex in the ^1H NMR spectrum, the ^1H NMR spectrum was recorded in CD_2Cl_2 revealing a peak at δ2.68 with integral of 3.0 that was assigned to the coordinated acetonitrile (free acetonitrile appears at δ1.99). The $^{31}P\{^1H\}$ NMR spectrum showed the coordinated ligand resonance at δ72.44 and an additional small signal which corresponded to the phosphorus signal of $[Co^{III}(\mathbf{PN})_2(H)(Cl)]^+$ suggesting chlorination by the solvent (Figure S16, see below). Comparative data for the free **PN** ligand are provided in the experimental section. The PH coupling constant of the hydride resonance is consistent with those of $[Co^{III}(2,2'\text{-bipy})(PEt_2Ph)_2H_2]^+$ with δ–21.7 $J_{cis\text{-H-P}}$ = 64 Hz (Table S1, Figure S1) and $[Co^{III}(triphos)(H)(MeCN)_2][PF_6]$ (triphos = 1,1,1-tris(diphenylphosphinomethyl)ethane) which shows δ–7.64 $J_{cis\text{-H-P}}$ = 65 Hz.[64]

$[Co^{III}(PN)_2(H)(Cl)][PF_6]$ (**3**). The cobalt(III) monohydride chloride (**3**) was identified by NMR spectroscopy, elemental analysis, ESI mass spectrometry and X-ray crystallography. The ^1H, $^{13}C\{^1H\}$ and $^{31}P\{^1H\}$ NMR spectra of **3** in solution showed sharp and well-resolved peaks with a similar pattern to that of **2**, consistent with mutually trans P atoms and C_2 symmetry (Figures S23-S31). A hydride signal appeared at δ–19.04 as a well-resolved triplet ($J_{cis\text{-H-P}}$ = 58.4 Hz). The ^{15}N chemical shift was determined by ^1H-^{15}N correlation as δ–96.5 compared to δ–1.6 for the free ligand.

The crystal structure of **3** (Figure 3) revealed a distorted octahedral geometry with the chloride ligand trans to a hydride and the two **PN** ligands arranged with mutually trans phosphorus atoms and mutually trans nitrogen atoms. The hydride was located by difference map and allowed to refine.

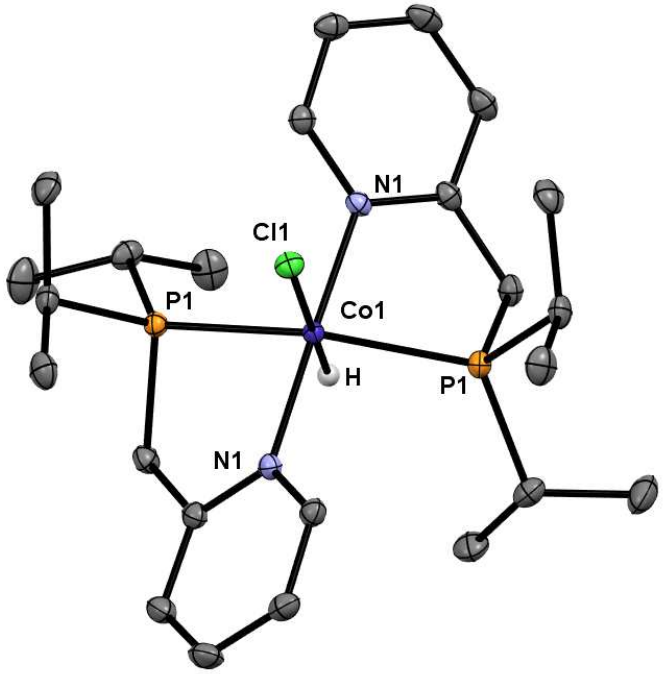

Figure 3. X-ray crystal structure of the cation of $[Co^{III}(\mathbf{PN})_2(H)(Cl)][PF_6]$ **3**. Selected hydrogen atoms and PF_6^- counter anion were removed for clarity. Thermal ellipsoids are shown with 50% probability. Co1-N1 1.9528(15), Co1-P1 2.2425(5), Co1-Cl1 2.3391(7), Co1-H1 1.54(7) Å, N1-Co1-P1 82.73(5), N1'-Co1-P1 96.43(5), N1-Co1-N1' 175.35(10), P1-Co1-P1' 159.32(3),Cl1-Co1-P1 100.339(15), Cl1-Co1-N1 92.32(5)°.

Reactivity of PN, 1, 2 and 3 towards CF_3CO_2H and H_2. Protonation of the **PN** ligand with trifluoroacetic acid (TFA, 10 equiv) resulted in a downfield shift of all the ^1H resonances; the largest shift of almost 1.0 ppm was recorded for the CH_2 resonance. The ^{31}P resonance moved from δ 12.4 to 32.1. This product is assigned as [**PNH**][O_2CCF_3] resulting from protonation of the pyridine nitrogen of **PN**. Reaction of **1** with TFA (10 equiv) in CD_3CN was followed by ^1H and ^{31}P NMR (Figures S33-S34). The product exhibited resonances with marginally different chemical shifts and almost identical coupling constants to those of $[\mathbf{PNH}]^+$ (Figure S9). The resonances were broadened by the paramagnetism of **1** and its products; the slight changes in chemical shift are also consistent with the paramagnetism. Thus we conclude that one (or less likely both) of the **PN** ligands of **1** has been protonated and dissociated as $[\mathbf{PNH}]^+$.

A similar study of the reaction of **2** with TFA (10 equiv) in CD_3CN generated a small amount of the same $[\mathbf{PNH}]^+$ product, but this did not increase with time and was attributed to the reaction of complex **1** present as an impurity in samples of **2**. Similar issues of Co(II) impurities in a Co(III) complex have been reported elsewhere.[56]

On leaving **3** in CD_3CN solution for 4 h at room temperature, the ^1H and ^{31}P-^1H NMR correlation spectra showed ca. 10% conversion of **3** to **2**. In a separate experiment, **3** was reacted with trifluoroacetic acid (10 equiv) in CD_3CN for 2 days at room temperature resulting in complete

conversion to **2**. The same result was achieved after 6 h with heating to 45 °C. The overall evidence indicates therefore, that **2** does not react with TFA under these conditions.

A reaction of **2** with H_2 (4 bar in CD_3CN) was performed anticipating formation of a dihydrogen complex. No such evidence was found but after 7.5 h at room temperature, the growth of broad resonances in the ^1H NMR spectrum and the decrease of the ^{31}P resonance relative to that of PF_6^- signaled reduction to **1**. Further formation of **1** ensued over the next 15 h.

Absorption properties. $[Co^{II}(\mathbf{PN})_2(MeCN)]^{2+}$ **1** shows one UV-vis absorption band in MeCN solution in the visible region centered at λ_{max} 448 nm (ε = 902 $M^{-1}\,cm^{-1}$) (Table 1, Figure 4). For comparison, $[Co^{II}(MeCN)_6][BF_4]_2$ exhibits a d-d transition at 490 nm (ε = 14 $M^{-1}\,cm^{-1}$) and the free **PN** ligand exhibits no absorption band above 300 nm. The molar absorptivity of $[Co^{II}(\mathbf{PN})_2(MeCN)]^{2+}$ is much larger than that of d-d transitions in Co(II) complexes with six- (< 50 $M^{-1}\,cm^{-1}$) or five-coordination (ranges from 50-300 $M^{-1}\,cm^{-1}$).[65, 66] The band at 450 nm of **1** is therefore assigned to a transition involving charge transfer to/from the **PN** ligand.

The UV-Vis absorption band of **2** in MeCN appears at λ_{max} = 413 nm (ε = 1640 $M^{-1}\,cm^{-1}$) and is assigned as a CT transition involving the Co(III) and pyridine ligands (Figure 4). A similar characteristic band was also observed in the visible absorption band of a family of $[Co^{III}(N4Py)X)]^{n+}$ complexes (see Chart SI for structure).[67] The corresponding band of **3** is found at 450 nm, a red shift of 37 nm with respect to **2**. None of these Co complexes showed significant emission at room temperature.

The reaction of **1** with 2.0 eq of TFA resulted in a decrease of absorbance at 450 nm consistent with ligand loss (see above). Subsequent addition of NEt_3 (2.0 eq) resulted in partial recovery of absorption (Figure S39).

Table 1. UV-Vis spectroscopic data of PN ligand and Co complexes in MeCN solution[a]

Compound	λ_{max} (nm)	ε ($M^{-1}\,cm^{-1}$)	Assignment	
PN ligand	260	4270	π-π^* (L)	This work
$[Co^{II}(MeCN)_6][BF_4]_2$	490	14	d-d	This work
1	448	902	CT	This work
2	413	1640	CT	This work
3	450	2200	CT	This work
$[Co^{III}(N4Py)(N_3)]^{2+}$	496	877	CT	67
$[Co^{III}(N4Py)(NCS)]^{2+}$	504	1140	CT	67

[a] The structures of the literature complexes are shown in Chart S1

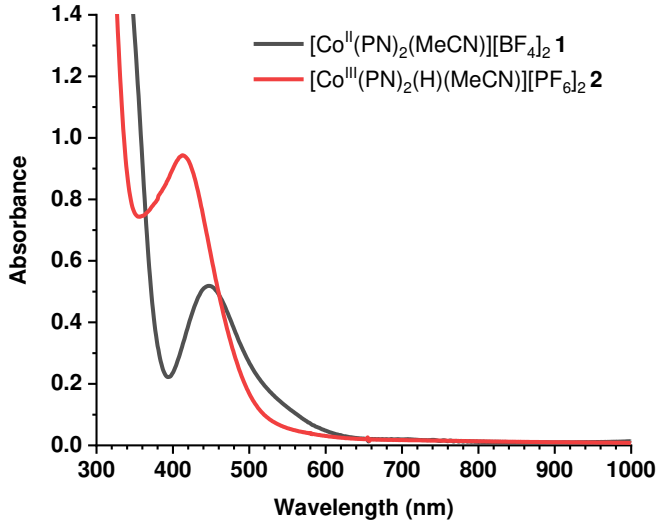

Figure 4. UV-vis absorption spectra of $[Co^{II}(\mathbf{PN})_2MeCN][BF_4]$ (**1**) and $[Co^{III}(\mathbf{PN})_2(H)(MeCN)][PF_6]_2$ (**2**), $5.75x10^{-4}$ M in CH_3CN.

Electrochemical properties. Data from cyclic voltammetry (CV) studies of complexes **1** – **3** are summarized in Table 2. The CV of **1** showed two reduction processes with a reversible wave at $E_{1/2}$ = –1.08 V (ΔE_p = 70 mV) and an irreversible wave at E_{pc} = –2.28 V (Table 2, Figure 5a). The first reversible redox wave was assigned to the Co(II/I) couple; the second wave is tentatively assigned to the Co(I/0) couple or possibly a ligand-centered reduction of $Co(I)L^{\bullet-}$. Moreover, the Co(II/I) redox couple was fully reversible upon scanning through a narrow potential window. The cathodic and anodic peak currents for the Co(II/I) redox wave of **1** increased linearly with the scan rate $\nu^{1/2}$ consistent with diffusion-controlled current (Figure S41). These data indicate that no ligand loss from **1** occurs following one electron reduction. On scanning to more positive potential, an irreversible process, assumed to be Co(III/II) was observed with oxidation at 0.65 V and a reductive peak at 0.0 V (Figure 5c).

Table 2. Electrochemical characterization data of 1-3[a]

Com-plex	$E_{1/2}$[b]/V (ΔE_p, mV)		E_{pc}[b]/V			E_{pa}[b]/V	
	$Co^{III/II}$	$Co^{II/I}$	$Co^{III/II}$	$Co^{II/I}$	$Co^{I/0}$ or $Co^{I}(L^{\bullet-})$	$Co^{III/II}$	$Co^{II/I}$
1	see text	–1.08 (70)	0.0	–1.43	–2.28		–0.73
2	–1.10 (110)	-	–1.14	–1.95	-	–1.03	–1.65
3	see text	see text	–1.48	–2.02		–1.10	–1.65

[a] [complex] = 1 mM, solvent MeCN, electrolyte 0.1 M $TBAPF_6$, scan speed 100 mV s^{-1};
[b] referenced internally to ferrocene.

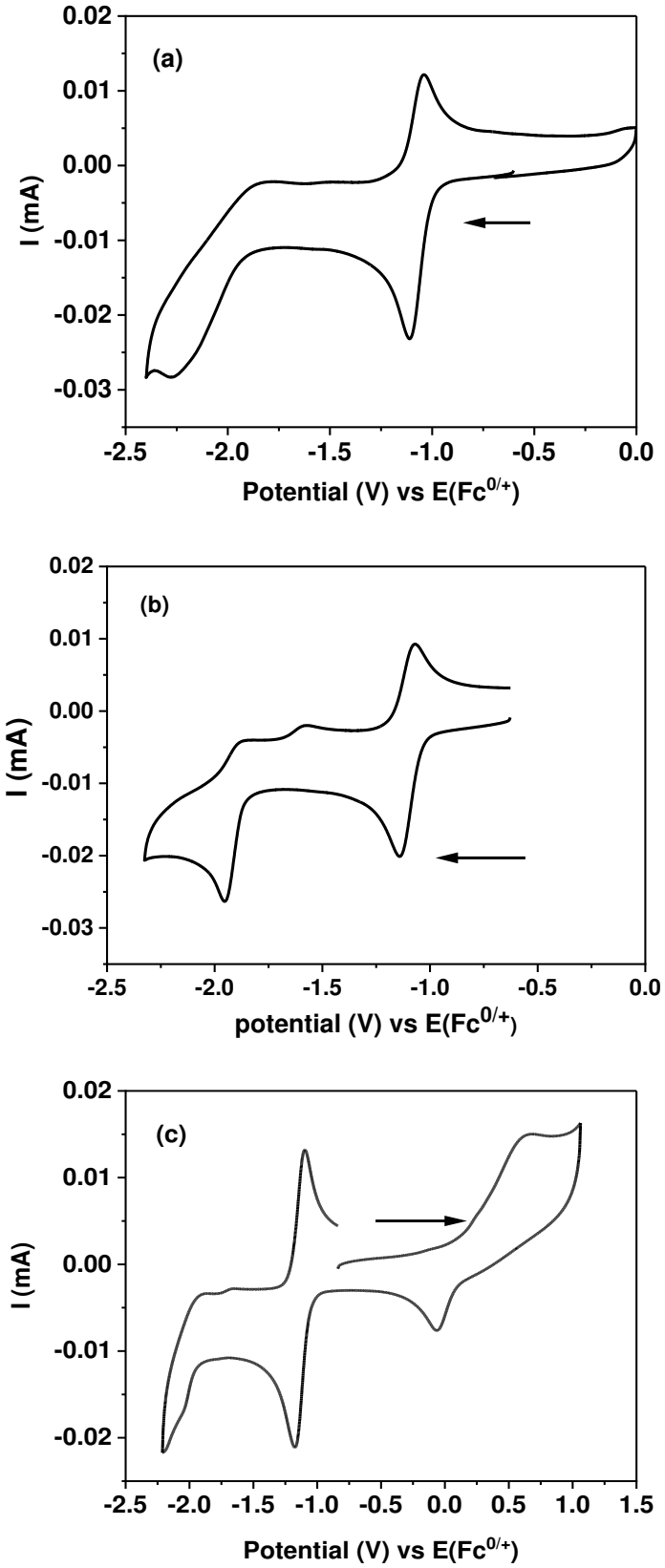

Figure 5. Cyclic voltammograms (a) reductive scan of **1**, (b) reductive scan of **2**, (c) initial oxidative scan of **1** followed by reductive scan. Conditions 1 mM complex in CH_3CN with 0.1 M $TBAPF_6$. All CVs in this paper are drawn with the IUPAC convention showing potentials increasing from negative to positive.

The dicationic complex **2** shows two reduction processes at –1.15 (Co(III/II)) and –1.95 V (Co(II/I)), where the Co(III/II) couple was quasi-reversible (ΔE_p 110 mV at 100 mV s^{-1} (Figure 5b). Plots of i_{pc} and i_{pa} of this couple as a function of $\nu^{1/2}$ again showed a linear dependence indicating diffusion-controlled current (Figure S41). For an ideal reversible one-electron transfer followed by a rapid irreversible chemical step (E_rC_i mechanism), a plot of E_{pa} or E_{pc} vs log ν gives a characteristic slope of $\Delta E_p / \Delta\log(\nu)$ of ±30 mV, respectively (Savéant's zone KP, moving to zone KO with increasing scan rate). [52,47,56, 68,69] For **2**, slopes of –31 mV and +29 mV, respectively, were obtained for the cathodic and anodic peak potentials of the Co(III)/(II) couple, respectively, with scan rates from 0.5 to 10 V s^{-1} (Figure S42). These data indicate the reversible reduction of **2** to $[Co^{II}(\mathbf{PN})_2(H)(MeCN)]^+$ followed by an irreversible chemical reaction (E_rC_i mechanism), consistent with dissociation of the MeCN ligand from the reduced Co(II)-H species. There has been much discussion in the literature about whether hydrogen is formed from metal hydrides by monometallic or bimetallic mechanisms.[20,70] A theoretical slope (ΔE_p/log ν) of 20 mV is expected for an ideal bimolecular reaction from plotting E_{pc} versus log ν,[14, 68] whereas our measured values are ca. 30 mV. Hydrogen can potentially be evolved by a bimetallic mechanism from reaction between two Co(II) hydride species giving a theoretical slope of 20 mV. Our data suggests that this mechanism is not operating under these conditions. This observation leads us to propose that hydrogen production follows the monometallic heterolytic pathway (see below).

The cyclic voltammogram of **3** exhibited two irreversible reduction peaks at E_{pc} –1.48 V and –2.02 V during the cathodic scan, tentatively assigned to the stepwise reduction of metal-centered Co(III)/(II) and Co(II)/(I) couples, respectively. The cathodic peak currents at the Co(III)/(II) potential increased linearly with the scan rate $\nu^{1/2}$, again indicating diffusion-controlled current (Figure S43). A plot of experimental values of E_{pc} versus log ν gave a slope of –49 mV (Figure S44). Therefore, the electron transfer to the Co(III/II) couple was assigned as a quasi-reversible electron transfer followed by irreversible Cl^- dissociation (E_qC_i mechanism).[30,56,47]

UV-vis spectroelectrochemistry of 2 and 3. Following CV studies, complexes **2** and **3** were investigated by UV-Vis spectroelectrochemistry (UV-Vis SEC) in MeCN containing 0.1 M $TBAPF_6$. One-electron reduction of $[Co^{III}(\mathbf{PN})_2(H)(MeCN)]^{2+}$ at –0.78 V relative to the pseudo reference electrode resulted in a slight change in absorption of the peak at 425 nm upon exhaustive electrolysis (Figure 6a).

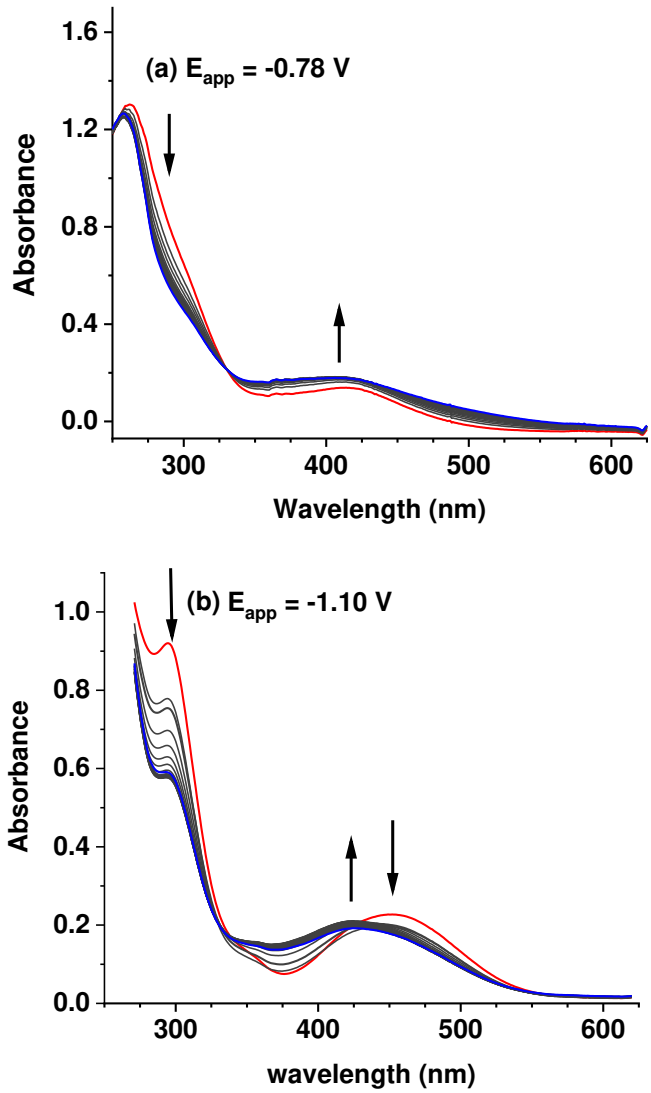

Figure 6. UV-Vis spectroscopic changes recorded during electrolysis of (a) **2** at E_{app} = –0.78 V relative to the pseudo reference electrode; (b) **3** at E_{app} = –1.10 V. (1 mM solutions in MeCN under an Ar atmosphere).

UV-Vis SEC of the monocation $[Co^{III}(\mathbf{PN})_2(H)(Cl)]^+$ of **3** in MeCN solution resulted in a blue shift of 25 nm during electrolysis at E_{app} = –1.10 V relative to the pseudo reference electrode (Figure 6b) generating a band in a similar, but not identical, position to that observed for **2**. Considering that reduction may not be complete and there may be equilibria with chloride, we tentatively deduce that reduction of either **2** or **3** leads to $[Co^{II}(\mathbf{PN})_2H]^+$ and that the latter may have MeCN as an additional ligand (Scheme 2).

Scheme 2. Mechanisms of reduction of 2 and 3 in CH_3CN from electrochemical studies

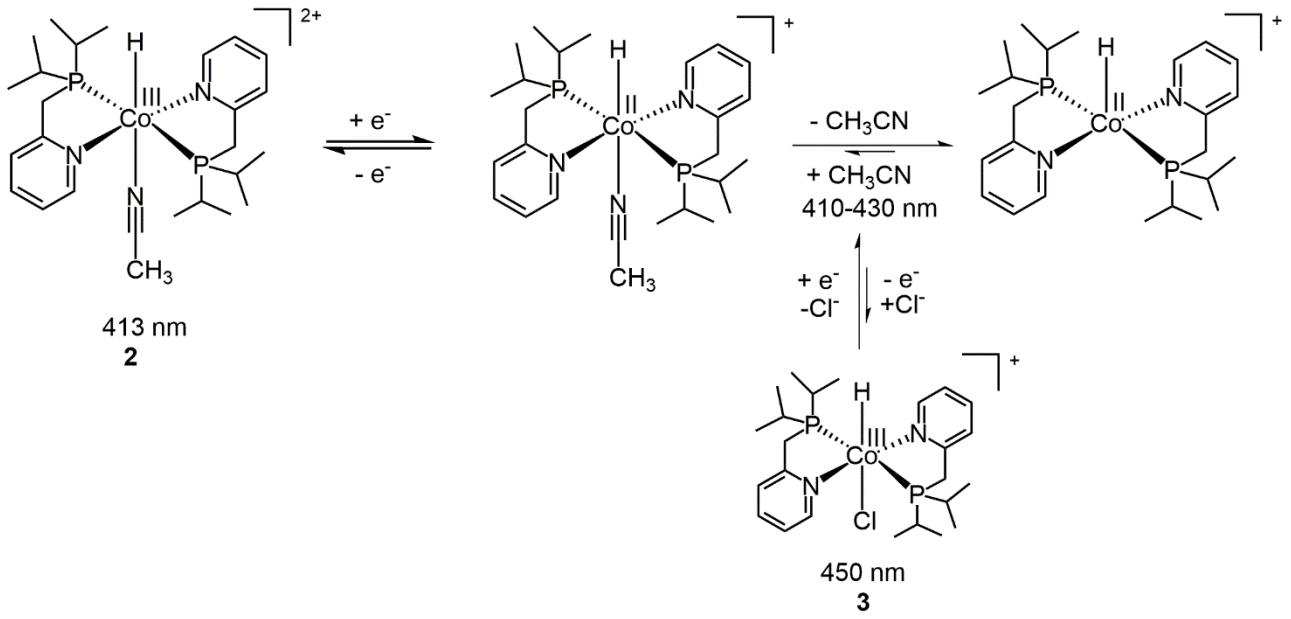

5

Electrocatalytic proton reduction to dihydrogen. On addition of trifluoroacetic acid (TFA) to **1**, the fully reversible Co(II/I) couple at –1.08 V became irreversible and catalytic enhancement of the current near to the Co(II/I) couple was observed (Figure 7a). An increase in current with [TFA] is consistent with catalytic proton reduction to form H_2, as was confirmed in bulk electrolysis experiments (see below). The potential at which the current reaches a maximum shifts linearly to more negative potential, indicating deviation from perfect Nernstian behavior.[48] The maximum catalytic current normalized to the non-catalytic peak current i_{cat}/i_p increases linearly with $[TFA]^{1/2}$ (Figure S48).

Addition of TFA to **2** resulted in a current increase at more negative potentials than the Co(III/II) couple at –1.14 V (Figure 7b). Once again, the potential of maximum current became more negative and i_{cat}/i_p increases linearly with $[TFA]^{1/2}$ (Figure S49). Comparison of **1** and **2** under catalytic conditions with 10 mM TFA showed overlap between the catalytic wave near to the Co(III/II) couple of **2** and the catalytic wave near to the Co(II/I) couple of **1** (Figure 8). This observation indicates that reduction of Co(III) to Co(II) is essential before H_2 can be generated.

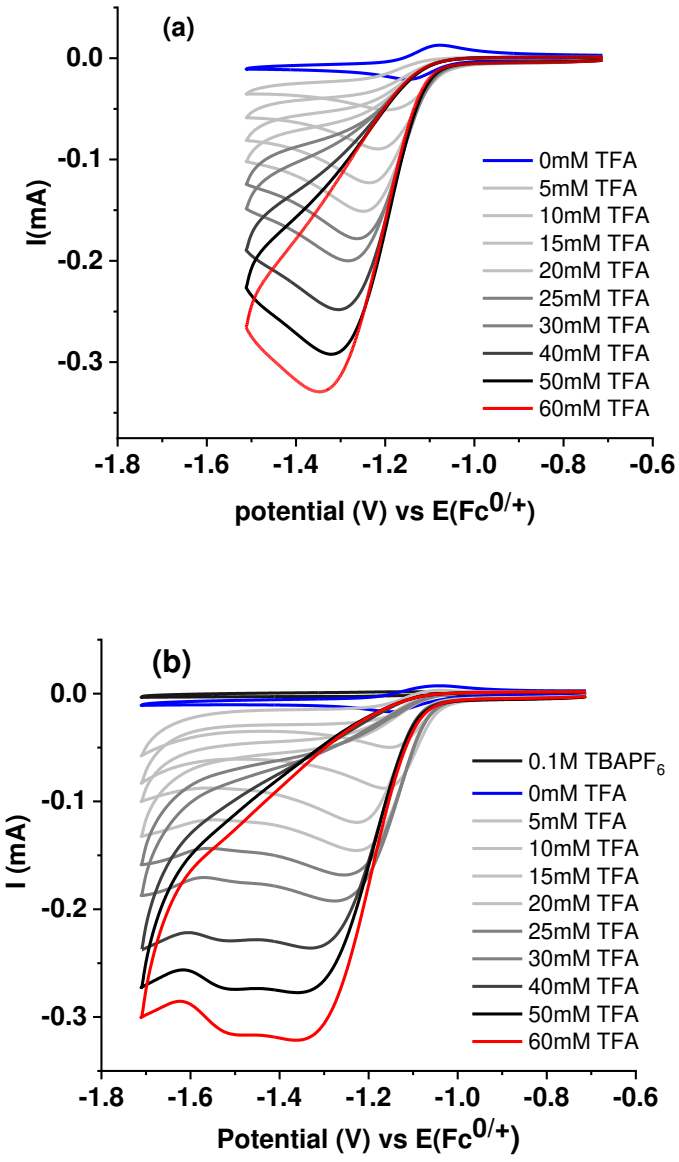

Figure 7. Effect of addition of TFA, (a) CVs of **1**; (b) CVs of **2**. Conditions: complex 1 mM in CH_3CN, with 0.1 M $TBAPF_6$ at scan rate of 100 mV s^{-1}.

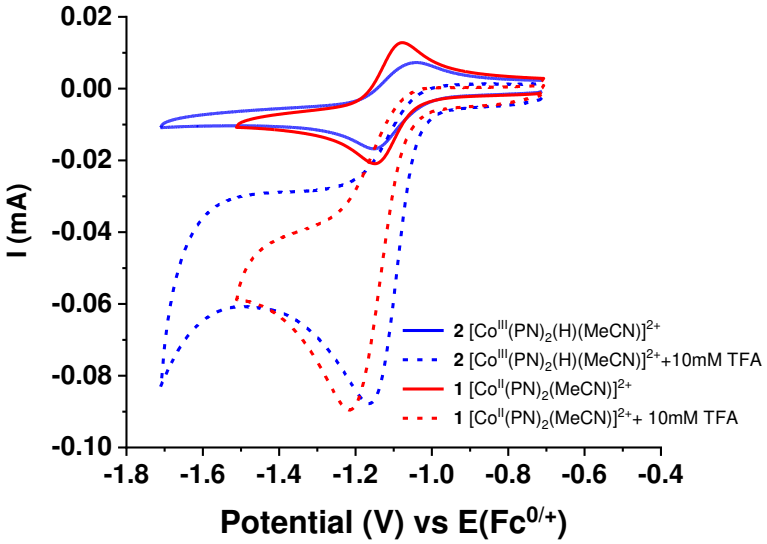

Figure 8. CVs of **2** (1 mM) in the absence and presence of 10 mM TFA in CH_3CN containing 0.1 M $TBAPF_6$ at a scan rate of 100 mV s^{-1}, compared to the CV of **1** under the same conditions.

Control experiments were also carried out using solutions of the Co(II) precursor $[Co(CH_3CN)_6][BF_4]_2$ and the **PN** ligand in the presence of 170 mM TFA in separate experiments, which showed negligible increases of current around –1.4 V confirming that electrocatalysis originates from **1** and **2**. A control experiment under bulk electrolysis conditions with $TBAPF_6$ (0.1 M) and TFA (60 mM) showed no catalytic current (Figure S54). However, free **PN** ligand was able to catalyze proton reduction at a more negative potential of –1.8 V (Figure S40).

The production of H_2 by bulk electrolysis. To confirm that the catalytic wave at ca. –1.4 V originated from H_2 evolution catalysis, bulk electrolysis experiments were performed for **1**-**3** in acetonitrile (Table 3). The amount of H_2 produced in the head space of the electrochemical cell after bulk electrolysis over 2 h was analyzed quantitatively by GC to obtain the Faradaic efficiency for hydrogen evolution, FE(H_2) (Figure S51). All three complexes gave efficiencies close to 100%. We used the value of $E^0_{H+/H2}$ = –0.028 V vs. $Fc^{0/+}$ in acetonitrile[71] in conjunction with TFA's p*K*a = 8.60 to determine the value of $E^0_{TFA/H2}$ = –0.77 V vs. E($Fc^{0/+}$). The overpotential (η) of each catalyst was determined using this value and the potential at the half-maximum current of the catalytic wave ($E_{cat/2}$) (Table 3).

The catalytic current was measured for 2 h during controlled potential electrolysis for complexes **1**-**3** (Figure S52, S55, S56). For **1**, the catalytic current decreased slightly over the period. For **2**, the current increases slightly over the first hour before stabilizing, while for **3** the corresponding increase in the first hour is more significant, consistent with initial loss of chloride. UV/vis spectra were measured before and after electrolysis with **3** (0.55 mM in 0.1 M $TBAPF_6$, 30

mM TFA CH_3CN). The spectra showed that **3** is stable in electrolyte with added acid for at least 1 h. During electrolysis, the color changed from bright orange to pale yellow, the absorption maximum shifted from 450 to 430 nm, and the absorbance decreased by 80% (Figure S57). This change is consistent with conversion of **3** to a mixture of different complexes, rather than simply conversion to **2**.

Table 3. Conditions for bulk electrolysis acidified with TFA.[a]

Complex	[TFA] mM	E_{cat} (V)	$E_{cat/2}$ (V)	E_{app} (V)	η (mV)	% FE(H_2)
1	60	–1.47	–1.21	–1.33	440	100
2	60	–1.46	–1.22	–1.40	450	91
3	30	–1.55	–1.34	–1.50	570	101

[a] Concentration of complex 0.9 mM in CH_3CN, 0.1 M $TBAPF_6$ electrolyte, $\eta = E_{cat/2}-E^0_{HA/H2}$, $E^0_{HA/H2}$ for TFA in MeCN = –0.77 V. E_{app} is the voltage applied during electrolysis

Furthermore, a dipping test was performed to prove that there is no deposition of catalytically active particles at the surface of the carbon plate used as the working electrode during bulk electrolysis. After bulk catalytic electrolysis, the working electrode was rinsed with MeCN prior to reuse in an electrolyte solution without catalyst (Figure S54). The absence of a catalytic current was consistent with homogeneous electrocatalytic H_2 evolution and the lack of Co nanoparticle deposition.[72, 73]

Catalytic mechanism. In the preceding sections, we have reported a series of observations that carry implications for the catalytic mechanism. The UV-Vis and NMR spectroscopic measurements indicated that **1** loses **PN** ligand(s) in the presence of TFA while **2** is stable. There is strong evidence that ligands such as **PN** are hemilabile.[77] We therefore postulate that **1** can be protonated at a nitrogen atom of a **PN** ligand prior to one-electron reduction under electrocatalytic conditions to give a tricationic species opening up the chelate ring. We conclude that **1** lies outside the catalytic cycle whereas **2** may lie within the cycle. By comparison of **1** (Co(II)) and **2** (Co(III)) under catalytic conditions, we also showed that reduction of Co(III) to Co(II) is essential before H_2 can be generated.

The resulting ECEC cycle, taken as a working hypothesis (Scheme 3), is labeled starting with protonation of **1** to form a pendant pyridinium ion. The E1 step reduces Co(II) to a Co(I) species still containing protonated pyridinium. This step is followed by a ligand-assisted proton transfer from pyridinium to Co resulting in generation of the Co-H bond of **2** and formal oxidation to Co(III),

the C1 step. Complex **2** is now reduced in the E2 step from Co(III) to Co(II). Finally, protonation by $2H^+$ generates H_2 in the C2 step and regenerates the initial ring-opened species. It is important to note that the cycle is complicated by equilibria between species with and without coordinated MeCN (see Scheme 2). The opening of the **PN** chelate to form a pyridinium plays an analogous role to the pendant amine in the $[Ni(P_2N_2)_2]^{2+}$ electrocatalysts.[17] The proton for the formation of **2** in the C1 step may be derived from the pyridinium or from the bulk solution.

Scheme 3. Proposed mechanism for electrocatalytic hydrogen evolution catalyzed by 1.

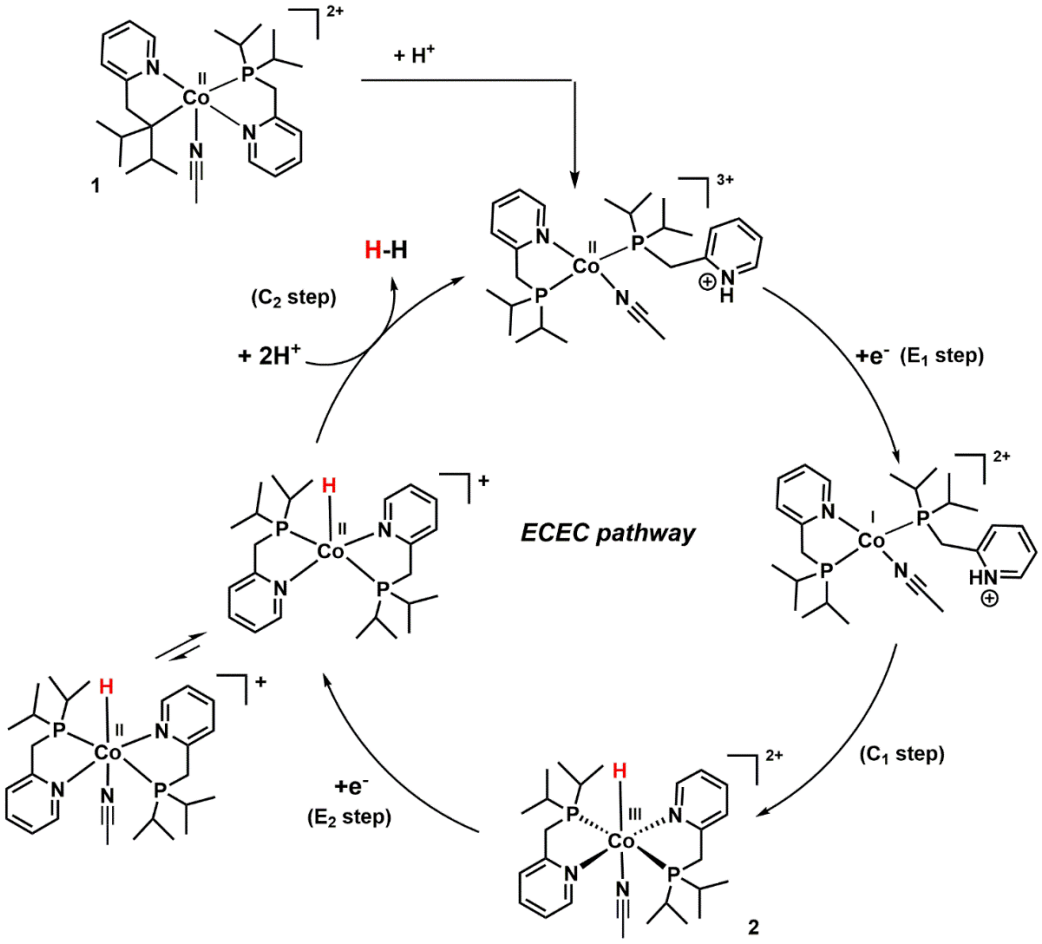

Further information testing this ECEC mechanism should be obtainable by Foot of the Wave Analysis (FOWA). Data from FOWA for **1** and **2** (Supporting Information) allow derivation of rate constants as a function of acid concentration and scan rate provided appropriate conditions are met. These nominal rate constants show a marked curvature with acid concentration indicative of the presence of two or more mechanisms. We associate this change in mechanism with change in speciation of the catalyst as [TFA] is increased. While Scheme 3 should be regarded as one likely mechanism, there is evidence that additional mechanisms occur.

CONCLUSION

The use of 2-(diisopropylphosphinomethyl)pyridine, **PN**, as a ligand enabled the synthesis of a group of cobalt complexes in +II and +III oxidation states with two **PN** ligands. The resulting $[Co^{II}(\mathbf{PN})_2(MeCN)][BF_4]_2$ **1**, $[Co^{III}(\mathbf{PN})_2(H)(MeCN)][PF_6]_2$ **2** and $[Co^{III}(\mathbf{PN})_2(H)(Cl)][PF_6]$ **3** all exhibit structures with mutually trans phosphorus and mutually trans nitrogen atoms, a geometry which we have not identified for Co complexes of neutral κ^2 P-N ligands in the CSD. The Co(II) salt **1** forms a square pyramidal geometry with axial MeCN in a low-spin electronic state, typical for a 17-e complex. At least one **PN** ligand of **1** is protonated and displaced in the presence of 10 equiv TFA. Although **2** is stable under these conditions, the chloride ligand of **3** is displaced by MeCN solvent in the presence of acid (or more slowly in MeCN alone) as a consequence of the trans influence of hydride. The Co(II/I) couple of **1** exhibits fully reversible electrochemistry in MeCN solution, while the Co(III/II) couple of **2** is quasi-reversible. Variable scan rate analysis and spectroelectrochemistry suggest that **2** loses MeCN on reduction. Complexes **1** and **2** catalyze proton reduction to hydrogen in the presence of TFA (solvent MeCN) with high Faradaic efficiency with an overpotential of ca. 450 mV and a peak catalytic current at ca. –1.3 V vs $E(Fc^+/Fc)$ corresponding to the Co(II/I) couple. A provisional catalytic cycle is proposed involving opening of the **PN** chelate ring on protonation of Co(II) allowing the resulting pyridinium to act as a pendant amine. However, Foot of the Wave Analysis indicates that more than one mechanism occurs, probably as a consequence of change in speciation with acid concentration. Complex **2** provides an example of a well-characterized cobalt hydride complex that is active in electrocatalysis of proton reduction. It points the way toward improved catalyst designs for catalysis.

ASSOCIATED CONTENT

Supporting Information.

The supporting information is available free of charge on the ACS Publications website at DOI:.
Structures of literature complexes, NMR data, magnetic data, UV/vis absorption spectra, other electrochemical data (PDF).
X-ray crystallographic information (CIF).

Accession Codes

CCDC 2021360 and 2021361 contain the supplementary crystallographic data for this paper. These data can be obtained free of charge via www.ccdc.cam.ac.uk/data_request/cif , or by emailing data_request@ccdc.cam.ac.uk, or by contacting The Cambridge Crystallographic Data Centre, 12 Union Road, Cambridge CB2 1EZ, UK; fax +44 1223 336033.

AUTHOR INFORMATION

Corresponding Authors

Richard E. Douthwaite – *Department of Chemistry, University of York, York YO10 5DD, UK*, Orcid.org/0000-0002-8423-7528, Email: richard.douthwaite@york.ac.uk

Robin N. Perutz - *Department of Chemistry, University of York, York YO10 5DD, UK*, Orcid.org/0000-0001-6286-0282, Email: robin.perutz@york.ac.uk

Authors

Khanittha Walaijai - *Department of Chemistry, University of York, York YO10 5DD, UK*

Stuart A. Cavill - *Department of Physics, University of York, York YO10 5DD, UK*

Adrian C. Whitwood - *Department of Chemistry, University of York, York YO10 5DD, UK*

Notes

The authors declare no competing financial interest

ACKNOWLEDGEMENTS

KW thanks the Development and Promotion of Science and Technology Talents Project (DPST), Thailand for financial support. We thank Philip Dyer and Claire Brodie (Durham University) for discussions and Raymond Fan, Diamond Light Source, for assistance with the magnetometry measurements. We are grateful to a reviewer for advice about Foot of the Wave Analysis.

REFERENCES

1. Dalle, K. E.; Warnan, J.; Leung, J. J.; Reuillard, B.; Karmel, I. S.; Reisner, E., Electro- and solar-driven fuel synthesis with first row transition metal complexes. *Chem. Rev.* **2019,** *119*, 2752-2875.

2. Roger, I.; Shipman, M. A.; Symes, M. D., Earth-abundant catalysts for electrochemical and photoelectrochemical water splitting. *Nat. Rev. Chem.* **2017,** *1*.

3. Kaeffer, N.; Chavarot-Kerlidou, M.; Artero, V., Hydrogen evolution catalyzed by cobalt diimine dioxime complexes. *Acc. Chem. Res.* **2015,** *48*, 1286-1295.

4. Bullock, R. M.; Helm, M. L., Molecular electrocatalysts for oxidation of hydrogen using earth-abundant metals: Shoving protons around with proton relays. *Acc. Chem. Res.* **2015,** *48*, 2017-2026.

5. Zhang, B. B.; Sun, L. C., Artificial photosynthesis: opportunities and challenges of molecular catalysts. *Chem. Soc. Rev.* **2019,** *48*, 2216-2264.

6. Evans, R. M.; Siritanaratkul, B.; Megarity, C. F.; Pandey, K.; Esterle, T. F.; Badiani, S.; Armstrong, F. A., The value of enzymes in solar fuels research - efficient electrocatalysts through evolution. *Chem. Soc. Rev.* **2019,** *48*, 2039-2052.

7. Lubitz, W.; Reijerse, E. J.; Messinger, J., Solar water-splitting into H_2 and O_2: design principles of photosystem II and hydrogenases. *Energ. Environ. Sci.* **2008,** *1*, 15-31.

8. Armaroli, N.; Balzani, V., Solar electricity and solar fuels: Status and perspectives in the context of the energy transition. *Chem. - Eur. J.* **2016,** *22*, 32-57.

9. Ardo, S.; Rivas, D. F.; Modestino, M. A.; Greiving, V. S.; Abdi, F. F.; Alarcon Llado, E.; Artero, V.; Ayers, K.; Battaglia, C.; Becker, J. P.; Bederak, D.; Berger, A.; Buda, F.; Chinello, E.; Dam, B.; Di Palma, V.; Edvinsson, T.; Fujii, K.; Gardeniers, H.; Geerlings, H.; Hashemi, S. M. H.; Haussener, S.; Houle, F.; Huskens, J.; James, B. D.; Konrad, K.; Kudo, A.; Kunturu, P. P.; Lohse, D.; Mei, B.; Miller, E. L.; Moore, G. F.; Muller, J.; Orchard, K. L.; Rosser, T. E.; Saadi, F. H.; Schuttauf, J. W.; Seger, B.; Sheehan, S. W.; Smith, W. A.; Spurgeon, J.; Tang, M. H.; van de Krol, R.; Vesborg, P. C. K.; Westerik, P., Pathways to electrochemical solar-hydrogen technologies. *Energ. Environ. Sci.* **2018,** *11*, 2768-2783.

10. Artero, V.; Chavarot-Kerlidou, M.; Fontecave, M., Splitting water with cobalt. *Angew. Chem. Int. Ed.* **2011,** *50*, 7238-7266.

11. Bacchi, M.; Berggren, G.; Niklas, J.; Veinberg, E.; Mara, M. W.; Shelby, M. L.; Poluektov, O. G.; Chen, L. X.; Tiede, D. M.; Cavazza, C.; Field, M. J.; Fontecave, M.; Artero, V., Cobaloxime-based artificial hydrogenases. *Inorg. Chem.* **2014,** *53*, 8071-8082.

12. Zhou, L. L.; Fu, L. Z.; Zhan, S. Z., Electro- and photo-chemical driven water reduction catalyzed by a cobalt(III) complex with high turnover number. *J. Mol. Catal. A* **2015,** *404*, 227-232.

13. Windle, C. D.; Kumagai, H.; Higash, M.; Brisse, R.; Bold, S.; Jousselme, B.; Chavarot-Kerlidou, M.; Maeda, K.; Abe, R.; Ishitani, O.; Artero, V., Earth-abundant molecular Z-scheme photoelectrochemical cell for overall water-splitting. *J. Am. Chem. Soc.* **2019,** *141*, 9593-9602.

14. Fang, M.; Wiedner, E. S.; Dougherty, W. G.; Kassel, W. S.; Liu, T.; DuBois, D. L.; Bullock, R. M., Cobalt complexes containing pendant amines in the second coordination sphere as electrocatalysts for H_2 production. *Organometallics* **2014,** *33*, 5820-5833.

15. Helm, M. L.; Stewart, M. P.; Bullock, R. M.; DuBois, M. R.; DuBois, D. L., A Synthetic Nickel Electrocatalyst with a Turnover Frequency Above 100,000 s^{-1} for H_2 Production. *Science* **2011,** *333*, 863-866.

16. Wiedner, E. S.; Appel, A. M.; DuBois, D. L.; Bullock, R. M., Thermochemical and mechanistic studies of electrocatalytic hydrogen production by cobalt complexes containing pendant amines. *Inorg. Chem.* **2013,** *52*, 14391-14403.

17. Klug, C. M.; Cardenas, A. J. P.; Bullock, R. M.; O'Hagan, M.; Wiedner, E. S., Reversing the tradeoff between rate and overpotential in molecular electrocatalysts for H_2 production. *ACS Catal.* **2018,** *8*, 3286-3296.

18. Cardenas, A. J. P.; Ginovska, B.; Kumar, N.; Hou, J.; Raugei, S.; Helm, M. L.; Appel, A. M.; Bullock, R. M.; O'Hagan, M., Controlling proton delivery through catalyst structural dynamics. *Angew. Chem. Int. Ed.* **2016,** *55*, 13509-13513.

19. Gross, M. A.; Reynal, A.; Durrant, J. R.; Reisner, E., Versatile photocatalytic systems for h_2 generation in water based on an efficient dubois-type nickel catalyst. *J. Am. Chem. Soc.* **2014,** *136*, 356-366.

20. Dempsey, J. L.; Brunschwig, B. S.; Winkler, J. R.; Gray, H. B., Hydrogen evolution catalyzed by cobaloximes. *Acc. Chem. Res.* **2009,** *42*, 1995-2004.

21. McKone, J. R.; Marinescu, S. C.; Brunschwig, B. S.; Winkler, J. R.; Gray, H. B., Earth-abundant hydrogen evolution electrocatalysts. *Chem. Sci.* **2014,** *5*, 865-878.

22. Darcy, J. W.; Koronkiewicz, B.; Parada, G. A.; Mayer, J. M., A continuum of proton-coupled electron transfer reactivity. *Acc. Chem. Res.* **2018,** *51*, 2391-2399.

23. Warren, J. J.; Tronic, T. A.; Mayer, J. M., Thermochemistry of proton-coupled electron transfer reagents and its implications. *Chem. Rev.* **2010,** *110*, 6961-7001.

24. Weinberg, D. R.; Gagliardi, C. J.; Hull, J. F.; Murphy, C. F.; Kent, C. A.; Westlake, B. C.; Paul, A.; Ess, D. H.; McCafferty, D. G.; Meyer, T. J., Proton-coupled electron transfer. *Chem. Rev.* **2012,** *112*, 4016-4093.

25. Bourrez, M.; Steinmetz, R.; Ott, S.; Gloaguen, F.; Hammarstrom, L., Concerted proton-coupled electron transfer from a metal-hydride complex. *Nat. Chem.* **2015,** *7*, 140-145.

26. Huang, T.; Rountree, E. S.; Traywick, A. P.; Bayoumi, M.; Dempsey, J. L., Switching between stepwise and concerted proton-coupled electron transfer pathways in tungsten hydride activation. *J. Am. Chem. Soc.* **2018,** *140*, 14655-14669.

27. Marinescu, S. C.; Winkler, J. R.; Gray, H. B., Molecular mechanisms of cobalt-catalyzed hydrogen evolution. *Proc. Natl. Acad. Sci. U. S. A.* **2012,** *109*, 15127.

28. Lacy, D. C.; McCrory, C. C. L.; Peters, J. C., Studies of cobalt-mediated electrocatalytic CO_2 reduction using a redox-active ligand. *Inorg. Chem.* **2014,** *53*, 4980-4988.

29. Rahman, A. F. M. M.; Jackson, W. G.; Willis, A. C.; Rae, A. D., Synthesis and crystal and molecular structure of a hydrido tetraamine cobalt(III) complex. *Chem. Commun.* **2003**, 2748-2749.

30. Wiedner, E. S.; Bullock, R. M., Electrochemical detection of transient cobalt hydride intermediates of electrocatalytic hydrogen production. *J. Am. Chem. Soc.* **2016,** *138*, 8309-8318.

31. Brewer, K. J.; Murphy, W. R.; Moore, K. J.; Eberle, E. C.; Petersen, J. D., Visible-light production of molecular hydrogen by sensitization of a cobalt dihydride complex. *Inorg. Chem.* **1986,** *25*, 2470-2472.

32. Camus, A.; Cocevar, C.; Mestroni, G., Cobalt complexes of 2,2'-bipyridine and 1,10-phenanthroline. *J. Organomet. Chem.* **1972,** *39*, 355-364.

33. Koelle, U.; Paul, S., Electrochemical reduction of protonated cyclopentadienylcobalt phosphine complexes. *Inorg. Chem.* **1986,** *25*, 2689-2694.

34. Elgrishi, N.; Kurtz, D. A.; Dempsey, J. L., Reaction parameters influencing cobalt hydride formation kinetics: Implications for benchmarking H_2-evolution catalysts. *J. Am. Chem. Soc.* **2017,** *139*, 239-244.

35. Bianchini, C.; Mealli, C.; Meli, A.; Peruzzini, M.; Zanobini, F., A stable eta-2-H_2 complex of cobalt - role of the H-H interaction in hydrogen transfer from metal to alkene. *J. Am. Chem. Soc.* **1988,** *110*, 8725-8726.

36. Heinekey, D. M.; van Roon, M., Dihydride complexes of the cobalt and iron group metals: An investigation of structure and dynamic behavior. *J. Am. Chem. Soc.* **1996,** *118*, 12134-12140.

37. Merz, L. S.; Blasius, C. K.; Wadepohl, H.; Gade, L. H., Square planar cobalt(II) hydride versus T-Shaped cobalt(I): structural characterization and dihydrogen activation with PNP-cobalt pincer Complexes. *Inorg. Chem.* **2019,** *58*, 6102-6113.

38. Ciancanelli, R.; Noll, B. C.; DuBois, D. L.; DuBois, M. R., Comprehensive thermodynamic characterization of the metal−hydrogen bond in a series of cobalt-hydride complexes. *J. Am. Chem. Soc.* **2002,** *124*, 2984-2992.

39. Guard, L. M.; Hebden, T. J.; Linn, D. E.; Heinekey, D. M., Pincer-supported carbonyl complexes of cobalt(I). *Organometallics* **2017,** *36*, 3104-3109.

40. Krishnan, V. M.; Arman, H. D.; Tonzetich, Z. J., Preparation and reactivity of a square-planar PNP cobalt(II)-hydrido complex: isolation of the first $\{Co\text{-}NO\}^8$-hydride. *Dalton Trans.* **2018,** *47*, 1435-1441.

41. Kuriyama, S.; Arashiba, K.; Tanaka, H.; Matsuo, Y.; Nakajima, K.; Yoshizawa, K.; Nishibayashi, Y., Direct transformation of molecular dinitrogen into ammonia catalyzed by cobalt dinitrogen complexes bearing anionic PNP pincer ligands. *Angew. Chem. Int. Ed.* **2016,** *55*, 14291-14295.

42. Wu, S. Q.; Li, X. Y.; Xiong, Z. C.; Xu, W. G.; Lu, Y. Q.; Sun, H. J., Synthesis and reactivity of silyl iron, cobalt, and nickel complexes bearing a PSiP -pincer ligand via Si-H bond activation. *Organometallics* **2013,** *32*, 3227-3237.

43. Suess, D. L. M.; Tsay, C.; Peters, J. C., Dihydrogen binding to isostructural S=1/2 and S=0 cobalt complexes. *J. Am. Chem. Soc.* **2012,** *134*, 14158-14164.

44. Tokmic, K.; Markus, C. R.; Zhu, L.; Fout, A. R., Well-defined cobalt(I) dihydrogen catalyst: experimental evidence for a Co(I)/Co(III) redox process in olefin hydrogenation. *J. Am. Chem. Soc.* **2016,** *138*, 11907-11913.

45. Artero, V.; Savéant, J.-M., Toward the rational benchmarking of homogeneous H_2-evolving catalysts. *Energ. Environ. Sci.* **2014,** *7*, 3808-3814.

46. Rountree, E. S.; McCarthy, B. D.; Eisenhart, T. T.; Dempsey, J. L., Evaluation of homogeneous electrocatalysts by cyclic voltammetry. *Inorg. Chem.* **2014,** *53*, 9983-10002.

47. Savéant, J. M., Elements of molecular and biomolecular electrochemistry : An electrochemical approach to electron transfer chemistry. Wiley: New York, 2006; pp 81-83.

48. Wang, V. C. C.; Johnson, B. A., Interpreting the electrocatalytic voltammetry of homogeneous catalysts by the foot of the wave analysis and its wider implications. *ACS Catal.* **2019,** *9*, 7109-7123.

49. Evans, D. F., The determination of the paramagnetic susceptibility of substances in solution by nuclear magnetic resonance. *J. Chem. Soc.* **1959**, 2003-2005.

50. Dolomanov, O. V.; Bourhis, L. J.; Gildea, R. J.; Howard, J. A. K.; Puschmann, H., OLEX2: a complete structure solution, refinement and analysis program. *J. Appl. Crystallogr.* **2009,** *42*, 339-341.

51. Sheldrick, G. M., Integrated space-group and crystal-structure determination. *Acta Crystallogr. Sect. A* **2015,** *71*, 3-8.

52. Sheldrick, G. M., Crystal structure refinement with SHELXL. *Acta Crystallogr. Sect. C* **2015,** *71*, 3-8.

53. Jansen, A.; Pitter, S., Synthesis of Hemilabile P,N Ligands: ω-2-Pyridyl-n-alkylphosphines. *Monatsh. Chem.* **1999,** *130*, 783-794.

54. Heintz, R. A.; Smith, J. A.; Szalay, P. S.; Weisberger, A.; Dunbar, K. R., Homoleptic transition metal acetonitrile cations with tetrafluoroborate or trifluoromethanesulfonate anions. In *Inorg. Synth.*, Coucouvanis, D., Ed. Wiley: New York, 2002; Vol. 33, pp 78-79.

55. We tested the proposed reduction protonation mechanism by reacting $Co(PN)_2Cl_2$ with KC_8 followed by protonation with $TsOH.H_2O$. This reaction generated **3** but in lower yield than by the original mechanism.

56. Wiedner, E. S.; Roberts, J. A. S.; Dougherty, W. G.; Kassel, W. S.; DuBois, D. L.; Bullock, R. M., Synthesis and electrochemical studies of cobalt(III) monohydride complexes containing pendant amines. *Inorg. Chem.* **2013,** *52*, 9975-9988.

57. Mague, J. T.; Hawbaker, S. W., 2-pyridylbis(diphenylphosphino)methane chemistry. Synthesis and structures of Cu(mu-eta(2):eta(1)$(Ph_2P)_2CHC_5H_4N)(THF)_2(BF_4)_2$ and $Ni(Ph_2PCH_2C_5H_4N)_2$ $NiCl_4$ $.0.85CH_2Cl_2$. *J. Chem. Crystallogr.* **1997,** *27*, 603-608.

58. Langer, R.; Gese, A.; Gesevicius, D.; Jost, M.; Langer, B. R.; Schneck, F.; Venker, A.; Xu, W. Q., Formation of different isomers of phosphine-imidazolyl and -pyridyl ruthenium(II) complexes affecting the catalyst activity in the acceptorless dehydrogenation of alcohols. *Eur. J. Inorg. Chem.* **2015**, 696-705.

59. Wei, S.; Pedroni, J.; Meißner, A.; Lumbroso, A.; Drexler, H.-J.; Heller, D.; Breit, B., Development of an improved rhodium catalyst for Z-selective anti-Markovnikov addition of carboxylic acids to terminal alkynes. *Chem. Eur. J.* **2013,** *19*, 12067-12076.

60. Atoh, M.; Kashiwabara, K.; Ito, H.; Ito, T.; Fujita, J., Preparation and characterization of $[CoX_2(Edpp)_2]^+$(Edpp=$NH_2CH_2CH_2P(C_6H_5)_2$, X=Cl^-, Br^-, I^-, NCO^-, NCS^-, N_3^-, O^{2-}) and $[CoX_2(En)(Dppe)]^+$(En=$NH_2CH_2CH_2NH_2$, Dppe=$(C_6H_5)_2PCH_2CH_2P(C_6H_5)_2$, X=$Cl^-$, Br^-, NCS^-) - Crystal-structures of trans(NCS,NCS),Cis(P,P)-$[Co(NCS)_2(Edpp)_2]Br.3H_2O.(CH_3)_2CO$ and cis-(NCS,NCS),Trans(P,P)-$[Co(NCS)_2(Edpp)_2]Br.CH_3OHCH$. *Bull. Chem. Soc. Jpn.* **1984,** *57*, 3139-3146.

61. Kita, M.; Kashiwabara, K.; Fujita, J.; Tanaka, H.; Ohba, S., Crystal-structures of trans-$[CoCl_2((CH_3)_2PCH_2CH_2P(CH_{3)2})_2]ClO_4$, trans-(Cl,Cl)CIS(P,P)-$[COCl_2(NH_2CH_2CH_2P(CH_3)_2)_2]PF_6.0.5CH_3OH$, and trans-$[COCl_2(NH_2CH_2CH_2NH_2)_2]NO_3$. *Bull. Chem. Soc. Jpn.* **1994,** *67*, 2457-2462.

62. Suzuki, T.; Fujiiwara, K.; Takagi, H. D.; Kashiwabara, K., Preparation and characterization of mixed-ligand cobalt(III) complexes containing (3-aminopropyl) dimethylphosphine (pdmp). Conformation of the six-membered pdmp chelate ring. *Dalton Trans.* **2007**, 308-319.

63. Fackler, J. P.; Fetchin, J. A.; Mayhew, J.; Seidel, W. C.; Swift, T. J.; Weeks, M., Chemical exchange in "virtually coupled" systems. Metal-ion-induced relaxation of methyl-phosphorus coupling in phosphine complexes. *J. Am. Chem. Soc.* **1969,** *91*, 1941-1947.

64. Marinescu, S. C.; Winkler, J. R.; Gray, H. B., Molecular mechanisms of cobalt-catalyzed hydrogen evolution. *Proceedings of the National Academy of Sciences* **2012,** *109*, 15127.

65. Sénèque, O.; Campion, M.; Giorgi, M.; Le Mest, Y.; Reinaud, O., Funnel complexes with CoII and NiII: New probes into the biomimetic coordination ability of the calix[6]arene-based tris(imidazole) system. *Eur. J. Inorg. Chem.* **2004,** *2004*, 1817-1826.

66. Chan, S. L.-F.; Lam, T. L.; Yang, C.; Yan, S.-C.; Cheng, N. M., A robust and efficient cobalt molecular catalyst for CO_2 reduction. *Chem. Commun.* **2015,** *51*, 7799-7801.

67. Lo, W. K. C.; Castillo, C. E.; Gueret, R.; Fortage, J.; Rebarz, M.; Sliwa, M.; Thomas, F.; McAdam, C. J.; Jameson, G. B.; McMorran, D. A.; Crowley, J. D.; Collomb, M.-N.; Blackman, A. G., Synthesis, characterization, and photocatalytic H_2-evolving activity of a family of $[Co(N4Py)(X)]^{n+}$ complexes in aqueous solution. *Inorg. Chem.* **2016,** *55*, 4564-4581.

68. Bard, A. J.; Faulkner, L. R., *Electrochemical Methods: Fundamentals and Applications*. Wiley: New York, 2001; Vol. 2, p. 499.

69. Lee, K. J.; Elgrishi, N.; Kandemir, B.; Dempsey, J. L., Electrochemical and spectroscopic methods for evaluating molecular electrocatalysts. *Nat. Rev. Chem.* **2017,** *1*.

70. Wiedner, E. S.; Chambers, M. B.; Pitman, C. L.; Bullock, R. M.; Miller, A. J. M.; Appel, A. M., Thermodynamic hydricity of transition metal hydrides. *Chem. Rev.* **2016,** *116*, 8655-8692.

71. Roberts, J. A. S.; Bullock, R. M., Direct determination of equilibrium potentials for hydrogen oxidation/production by open circuit potential measurements in acetonitrile. *Inorg. Chem.* **2013,** *52*, 3823-3835.

72. Kaeffer, N.; Morozan, A.; Fize, J.; Martinez, E.; Guetaz, L.; Artero, V., The dark side of molecular catalysis: Diimine–dioxime cobalt complexes are not the actual hydrogen evolution electrocatalyst in acidic aqueous solutions. *ACS Catal.* **2016,** *6*, 3727-3737.

73. Elgrishi, N.; McCarthy, B. D.; Rountree, E. S.; Dempsey, J. L., Reaction pathways of hydrogen-evolving electrocatalysts: Electrochemical and spectroscopic studies of proton-coupled electron transfer processes. *ACS Catal.* **2016,** *6*, 3644-3659.

74. Wiedner, E. S.; Brown, H. J. S.; Helm, M. L., Kinetic analysis of competitive electrocatalytic pathways: New insights into hydrogen production with nickel electrocatalysts. *J. Am. Chem. Soc.* **2016,** *138,* 604-616.

75. Costentin, C.; Savéant, J.-M., Multielectron, multistep molecular catalysis of electrochemical reactions: Benchmarking of homogeneous catalysts. *ChemElectroChem* **2014,** *1*, 1226-1236.

76. Du, P.; Eisenberg, R., Catalysts made of earth-abundant elements (Co, Ni, Fe) for water splitting: Recent progress and future challenges. *Energ. Environ. Sci.* **2012,** *5*, 6012-6021.

77. Slone, C. S.; Weinberger, D. A.; Mirkin, C. A., The transition metal coordination chemistry of hemilabile ligands. In *Progress in Inorganic Chemistry, Vol 48*, Karlin, K. D., Ed. Wiley: New York, 1999; Vol. 48, pp 233-350.

For Table of Contents Only

Reactions of simple cobalt salts with phosphinopyridine ligands generate a square pyramidal, low spin Co(II) complex and two cobalt(III) hydride complexes that all catalyze reduction of protons from trifluoroacetic acid. The methodology allows direct association of the hydride complexes with the catalytic mechanism.